Marine Pollution Bulletin 193 (2023) 115082

Contents lists available at ScienceDirect

Marine Pollution Bulletin

journal homepage: www.elsevier.com/locate/marpolbul

The distribution and enrichment of trace elements in surface and core sediments from the Changjiang River Estuary, China: Evidence for anthropogenic inputs and enhanced availability of rare earth elements (REE)

Xiaoyu Zhang [a,b,*], Wen Du [c], Zhijie Xu [a], Andrew B. Cundy [d], Ian W. Croudace [d], Weiyan Zhang [e], Haiyan Jin [e], Jianfang Chen [e]

[a] School of Earth Sciences, Zhejiang University, Hangzhou 310027, China
[b] Hainan Institute of Zhejiang University, Sanya 572000, China
[c] South China University of Technology, Guangzhou 511442, China
[d] GAU-Radioanalytical, School of Ocean and Earth Science, National Oceanography Centre (Southampton), University of Southampton, Southampton SO14 3ZH, UK
[e] Key Laboratory of Marine Ecosystem and Biogeochemistry, State Oceanic Administration and Second Institute of Oceanography, Ministry of Natural Resources, Hangzhou 310012, China

ARTICLE INFO

Keywords:
Changjiang River Estuary
Trace elements
Elevated content
Anthropogenic input
Availability of REE

ABSTRACT

Huge amount of trace metals emitted through manmade activities are carried by the Changjiang River into the East China Sea. Most of them deposit in the Changjiang River Estuary and threaten the regional aquatic environment. In this study, major and trace elements of 34 archive surface sediments and two cores are examined. Sequential extraction procedures were also performed on surface sediments from 12 sites. We found that Tl, Tm, Er show distinct accumulation in surface sediments in the order of Tm > Tl > Er. Particularly, abnormally elevated HREE are observed mainly in those sites near the mouth of the estuary. Most elements exhibit an obvious reduction in the upper 30 cm of core B8, reflecting a decrease of sediment discharge from Changjiang River runoff. The increase of some trace elements recorded in the upper 20 cm of core C3 demonstrates a distinct local anthropogenic input in recent years.

1. Introduction

The Changjiang River Estuary (CRE) is the largest estuary, and the Changjiang River Delta (CRD) economic circle is one of the most developed regions in China. Rapid economic development and population growth in the CRD has led to large amounts of industrial effluent and municipal sewage being discharged into the CRE by Changjiang Diluted Water (CDW). The presence of harbors, petrochemical industries and shipyards results in the direct discharge of sewage and effluents to the estuary, with further effluents derived from industrial, urban and agricultural inputs along the coast of the city of Shanghai, Jiangsu and Zhejiang Provinces (Du et al., 2019; Duan et al., 2019; Guo and Yang, 2016; Wang et al., 2020; Yang et al., 2009), which have caused enhanced inputs of metallic and nonmetallic contaminants to the East China Sea (ECS). Previous studies on the pollution history of harmful heavy metals and As in the sediments of the CRE have revealed three chronological stages with different pollution levels before 2009 (Wang, 2008). Stage I spans from the end of the 1970s to the end of the 1980s, and is characterized by a high content of heavy metals. Stage II is from the very late 1980s to the early 1990s, with reduced metals in comparison with stage I, which may be due to the effective implementation of national policies of soil and water conservation since 1988. The subsequent Stage III records an abrupt increase of metal contamination until 2003. Construction of the Three Gorges Dam (TGD), the severe flood of the Changjiang River in 1998, and increasing emissions of industrial and domestic sewage from rapid industrial development may be responsible for increased contaminant concentrations in this stage. However, the impact of the drastic reduction in sediment discharge in the Changjiang River following water storage in the TGD, and the implementation of the 12th five year plan of "comprehensive prevention

* Corresponding author at: School of Earth Sciences, Zhejiang University, Hangzhou 310027, China.
E-mail address: Zhang_xiaoyu@zju.edu.cn (X. Zhang).

https://doi.org/10.1016/j.marpolbul.2023.115082
Received 6 November 2022; Received in revised form 5 April 2023; Accepted 17 May 2023
Available online 21 June 2023

and control of heavy metal pollution" in 2011, means that anthropogenic metal, metalloid and non-metal pollutant inputs may have reduced substantially after 2009, although this is not well-constrained currently and needs further investigation.

To date, studies on trace elements in the sediments of the CRE have mainly focused on those heavy metals (As, Cd, Cr, Cu, Pb, Hg, Ni, Zn, etc.) which are present in the EPA's[1] Priority Pollutants list (Guo and Yang, 2016; Hao et al., 2008; He et al., 2019; Hu et al., 2022; Li et al., 2019; Liu et al., 2016, 2019). Recently, however, more and more reports of abnormally elevated contents of trace elements which are not included in the EPA's Priority Pollutants list such as (Co, Ge, Mn, Sn, Te, Tl, V, U) (de Souza Viana et al., 2023; Duan et al., 2014; Fiket et al., 2018; Kimbrough et al., 2010; Zhuang et al., 2019). Besides, for the wide usage of fertilizer phosphorite and the rapid development of clean energy industry, rare earth elements (REE) (Borrego et al., 2004; de Oliveira et al., 2007; El Zrelli et al., 2021; Kulaksiz and Bau, 2007; Piarulli et al., 2021; Trifuoggi et al., 2018; Z. Wang et al., 2022) and even platinum group elements (PGE) (Dubiella-Jackowska et al., 2009; Essumang et al., 2010; Essumang and Adokoh, 2011; Komendova, 2020; Monteiro et al., 2017; Song et al., 2020) have been made for water and sediments in estuaries and coastal zones worldwide, with increasing recognition of the potential toxicity risk that this poses. Realizing the potential ecological risk from these unlisted trace elements, particularly from long exposures at low dose, China's 12th 5-year plan of "integrated prevention and control of heavy metal pollution" requires that the heavy metals Pb, Hg, Cd, Cr (and the metalloid As) are controlled as a priority, and that additionally Ni, Cu, Zn, Ag, V, Mn, Co, and Tl are monitored for key regions. Given (a) the particle reactivity and potential for sedimentary accumulation of many of these elements, and (b) the lack of published data on their concentration and distribution in the CRE, here we examine their distribution and enrichment in surface and core sediments, along with those of a range of other elements which may be input from regional and local contaminant sources, across the main suspended sediment mixing zone of the CRE system. The potential impact from the reduced discharge of CDW due to the construction of the TGD is then considered. To perform this aim, in this study, concentrations of 25 trace elements, and 15 rare earth elements are measured and presented from surface sediments from 34 sites (collected in 2006), and two sediment cores of 2 m length. Geo-accumulation indices are used to evaluate the contamination level and ecological risk of the estuarine sediments caused by the different trace elements. These data, with those of 11 major elements, grain size, and Loss on ignition (LOI), are also used in inter-elemental correlation, cluster analysis and Principle Component Analysis (PCA) to derive information on material sources and factors impacting the distribution of metals with abnormally elevated concentrations in the study area. Sequential extractions are performed to examine element exchangeability/availability and sediment interactions. The depositional history of trace elements is examined in the two sediment cores based on ^{210}Pb and ^{137}Cs dating, and its relationship to historical changes in the CRE assessed.

With a special focus on some rarely monitored metals, their abnormal accumulation and occurrence forms in the sediments, this study attempts to determine the key factors impacting the distribution and accumulation of trace elements in the study area, which will be beneficial for policy making on environment management and protection in the CRE, and also for understanding anthropogenic controls on trace element biogeochemical cycles in a heavily-industrialized, rapidly developing, large estuarine system.

[1] EPA: Environmental Protection Agency.

2. Study area and sampling

2.1. Geological background

The Changjiang River is the longest river in China, at 6300 km in length. The annual average runoff is 9051×10^8 m^3, and the discharge of suspended sediment is 4.33×10^8 t/year, varying between 3.41×10^8 t/year and 6.78×10^8 t/year (Datong station) (http://www.cjh.com.cn/, Changjiang Water Resources Commission, China). Sedimentary material from the Changjiang River Basin carried by Changjiang River runoff, combined with eroded material from the Old Yellow River Delta (OYRD), has a profound impact on sedimentation in the continental shelf of the ECS. Usually, after entering the ECS, CDW turns to the northeast and spread around 122.5°E (Chang et al., 2014), terrigenous material from both the Changjiang River Basin and Yellow River Basin has been reported in sediment as far as 127°E (X. Zhang et al., 2009), due to the complex interaction between different water masses. The hydrodynamic setting of the study area is shown in Fig. S1 (refer to Su and Yuan, 2005).

The sediment in the study area is mainly sand, with patchy distribution of clays and silts from the CRE to the Cold Eddy western to Cheju Island, as shown in Fig. 1. The clayey silt areas, where B8 and C3 are located, form at the convergence zones of fine sediment, and are suitable fields for studies of sedimentology procedure and marine environment evolution.

2.2. Sampling

In this study, 35 box surface sediments were collected at 34 sites (a duplicate sample was taken at the Z-18 site and named Z-35 in this paper) over the region 29.5–32°N, 120–127.5°E (covering the CRE and its adjacent sea area). Surface sediments were collected during cruises in summer 2006. Two, 2 m-long, sediment cores were collected during the 2016 summer cruise of Long-term observation and Research-plan in Changjiang Estuary (LORCE). The locations of the sampling stations are shown in Fig. 1. The samples were preserved in clean polyethylene bags at 4 °C after collection, prior to laboratory analyses.

3. Experiment and methods

3.1. Measurement items

Measurement of bulk surface sediments for major element concentrations (Na_2O, MgO, Al_2O_3, SiO_2, P_2O_5, K_2O, CaO, TiO_2, MnO, TFe_2O_3), the concentrations of 25 trace elements (including Sc, V, Cr, Co, Ni, Cu, Zn, Ga, As, Rb, Sr, Zr, Nb, Mo, Cd, Sn, Cs, Ba, Hf, Ta, W, Tl, Pb, Th, U) and 15 rare earth elements (REY: La, Ce, Pr, Nd, Sm, Eu, Gd, Tb, Dy, Ho, Er, Tm, Yb, Lu and Y), and Loss of Ignition (LOI) were carried out at the ALS Minerals-ALS Chemex facility in Guangzhou, China. Major elements (SiO_2, TiO_2, Al_2O_3, Fe_2O_3, MnO, MgO, CaO, K_2O, Na_2O, P_2O_5, and S), trace elements (As, Ba, Ce, Co, Cr, Cu, La, Nb, Ni, Pb, Rb, Sc, Sr, Zr, V, Ga, Sn, W, Y, Zn), and anions (Cl^-, Br^-, I^-) in B8 and C3 core sediments were determined at the National Oceanography Centre (Southampton), UK, where ^{210}Pb dating was also performed. To keep consistency with the elements measured for the surface sediments, B8 core sediments were analyzed for the same elements as the surface sediments at the ALS Minerals - ALS Chemex facility. However, due to the exhaustion of samples in some core layers, the measurements for B8 at the ALS Minerals - ALS Chemex facility were performed on adjacent depth increments. 12 box surface sediments near shore were selected, and an improved BCR three-stage sequential extraction performed on these samples to obtain information on the sediment associations and exchangeability of trace elements.

3.1.1. Major, trace elements and REY measurements

For major element analyses, concentrations were determined by X-

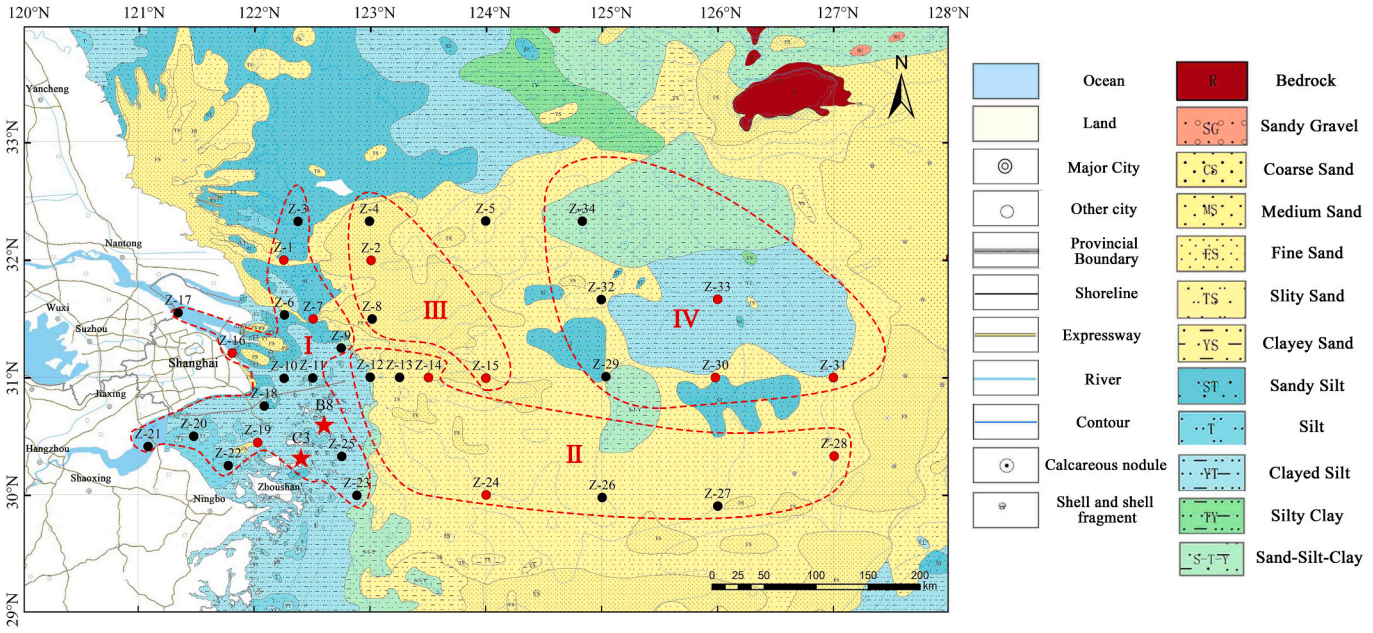

Fig. 1. The base map showing the distribution of sediment types in the study area referenced from sediment type map of the East China Sea (Shi, 2021) with sampling locations (● (●): Represents sampling station of surface sediment, among them, ●: Represents surface sediments which were performed with sequential extraction; ★: Represents sampling station of core sediment.; area in the red dotted curves represent the four sedimentary zones: I represents the Changjiang River Estuary and Hangzhou Bay, II represents the East China Sea shelf, III represents the tidal sand ridge of the Yangtze shoal, IV represents the interridge depression of tidal current sand). (For interpretation of the references to color in this figure legend, the reader is referred to the web version of this article.)

ray Fluorescence (XRF) at both laboratories. The accuracy of the analytical results is better than accuracy control relative error (RE) of 5 %, and the precision control relative deviation (RD) is 10 %.

At the ALS Minerals-ALS Chemex facility, trace elements were analyzed by Inductively Coupled Plasma Optical Emission Spectrometry, ICP-OES. The ignited sample powder was dissolved in HNO_3-$HClO_4$-HF-HCl and evaporated until dry. The residue was dissolved with diluted HCl, and then concentrations were measured using a Varian VISTA ICP-AES. Accuracy control relative error (RE) is 10 %, precision control relative deviation (RD) is 10 %. For rare earth elements, Inductively Coupled Plasma Mass Spectrometry, ICP-MS analysis was adopted in this study. The ignited sample powder was mixed with $LiBO_2/Li_2B_4O_7$ flux, fused at over 1025 °C, refrigerated and dissolved with HNO_3-HCl-HF. The concentrations were then determined using a Perkin Elmer Elan 9000 ICP-MS. Accuracy control relative error (RE) is 10 %, precision control relative deviation (RD) is 10 %. Besides, by heating the powdered samples to 1000 °C for over 2 h, the LOI was determined through weighing the mass loss after heating (GT/T14506-2019). The detection limit is >0.01 %.

At the National Oceanography Centre (Southampton), sediments were pelletised for trace element determinations and fused for major element determinations, and subsequently analyzed by WD-XRF using a Philips Magix-Pro WD-XRF fitted with a 4 kW Rh target X-ray tube. The methods used are well-established and are detailed by Croudace and Williams-Thorpe (1988). Precision is nominally 1 % rsd for major elements and 5 % rsd for trace elements. Accuracy was assessed by comparing a range of reference sample determinations (e.g. USGS MAG-1) with recommended values and was generally within 10 % of the working values quoted in the literature.

Comparisons of repeated measurements of major and trace elements for B8 core sediments from the two laboratories were carried out (in Supplementary materials). Most measurements are in the same range and trends in elements are similar, especially for the sudden change in element composition at 110-130 cm depth and 0-40 cm, as shown in Fig. S2.

3.1.2. ^{210}Pb radionuclide determinations

Total ^{210}Pb was determined via its grand-daughter ^{210}Po (proxy method of Flynn, 1968) which was leached from 3 g sediment sub-samples with aqua regia after addition of 50 μL ^{209}Po yield tracer (0.2 Bq/mL). The leachates were evaporated to dryness, re-dissolved in 1 M HCl and auto deposited on silver discs before counting for 2 days using Octete alpha spectrometry systems (Ortec, Oak Ridge, TN) in the GAU-Radioanalytical Laboratories, University of Southampton. Precision was <5 %. The ^{137}Cs activity of selected sub-samples was determined using a Canberra well-type HPGe gamma-ray spectrometer (Mirion UK Ltd., Didcot), counting for 100000 s. Detection limits were ca.1 Bq/kg.

3.1.3. Grain size analysis of surface sediments

Grain size was measured in the Key Laboratory of Submarine Geosciences, Second Institute of Oceanography, China. The samples were pretreated with 30 % H_2O_2 and 1 mol L^{-1} HCl to remove organic matter and carbonates, respectively. The treated samples were then measured using a "Mastersizer 2000" laser diffraction particle analyzer. The measurement repeatability error was <3 %.The average particle size, the standard deviation, the kurtosis, and the skewness coefficient were calculated according to the Folk and Ward nomenclature and classification system (Folk and Folk, 1957).

3.1.4. Sequential extraction experiment

The optimized method of BCR SE was adopted to determine extractable trace element contents of the sediments (Quevauviller et al., 1997; Rauret et al., 1999; Ure et al., 1993). The fractions determined and corresponding extract reagent used are listed as follows: (i) 0.11 M CH_3COOH is used to obtain the exchangeable or acid-extractable fraction; (ii) the reducible fraction is extracted with 0.5 M NH_2OH·HCl; (iii) the oxidizable fraction is extracted with 8.8 M H_2O_2/1 M CH_3COONH_4; (iv) the residual fraction is determined from the total quantities minus the three above fractions. The major and trace elements (Li, Na, Mg, Al, K, Ca, Sc, Ti, V, Cr, Mn, Fe, Co, Ni, Cu, Zn, Rb, Sr, Y, Zr, Nb, Mo, Cd, Sn, Cs, Ba, Hf, Ta, Pb, Th, U, As, La, Ce, Pr, Nd, Sm, Eu, Gd, Tb, Dy, Ho, Er, Tm, Yb, Lu, Tl) in different fractions were measured in ICP-MS at the

Table 1
Descriptive statistics of concentrations of elements in this study.

	Eigenvalue	SiO_2/%	TiO_2/%	Al_2O_3/%	Fe_2O_3/%	MnO/%	MgO/%	CaO/%	K_2O/%	Na_2O/%	P_2O_5/%
Surface	Min	48.55	0.36	8.78	3.00	0.04	1.18	2.58	2.02	1.08	0.07
	Max	73.32	0.88	16.61	19.16	0.34	2.99	11.65	3.23	2.30	0.36
	Mean	62.07	0.66	12.32	5.31	0.10	2.12	4.55	2.49	1.91	0.12
	Median	63.52	0.68	11.82	4.77	0.09	2.11	4.06	2.44	2.01	0.11
	SD	6.14	0.14	2.34	2.61	0.06	0.51	1.69	0.33	0.26	0.05
Core	Min	53.51	0.86	14.81	5.11	0.10	2.71	2.77	3.00	1.41	0.09
	Max	57.26	0.98	16.75	6.64	0.14	3.62	4.75	3.62	1.75	0.12
	Mean	55.90	0.92	16.11	6.12	0.12	3.25	3.61	3.36	1.58	0.10
	Median	55.98	0.92	16.25	6.23	0.12	3.28	3.27	3.37	1.59	0.10
	SD	0.90	0.03	0.46	0.38	0.01	0.27	0.74	0.17	0.08	0.01

	Eigenvalue	As/10^{-6}	Ba/10^{-6}	Cd/10^{-6}	Ce/10^{-6}	Co/10^{-6}	Cr/10^{-6}	Cs/10^{-6}	Cu/10^{-6}	Dy/10^{-6}	Er/10^{-6}
Surface	Min	3.90	393.00	0.02	50.80	7.50	40.00	2.62	6.00	2.91	1.53
	Max	21.00	469.00	0.15	99.60	18.70	93.00	12.85	43.50	5.03	2.98
	Mean	10.16	430.51	0.07	72.85	13.66	72.83	7.39	20.99	4.28	2.44
	Median	9.80	430.00	0.07	74.20	12.90	71.00	7.06	17.60	4.48	2.52
	SD	4.07	17.06	0.04	9.61	2.95	16.52	2.82	12.05	0.64	0.40
	BGV	7.70	412.00	0.07	67.00	12.00	61.00	6.30	15.00	3.42	1.50
Core	Min	6.20	490.60	0.07[a]	65.70	30.80	99.10	11.80[a]	19.50	5.16[a]	3.03[a]
	Max	12.60	547.60	0.12[a]	112.10	40.10	130.30	13.50[a]	36.40	5.60[a]	3.38[a]
	Mean	9.12	514.59	0.09[a]	83.28	36.51	112.91	12.95[a]	26.79	5.41[a]	3.17[a]
	Median	8.65	510.45	0.09[a]	81.70	36.80	113.10	13.00[a]	26.20	5.44[a]	3.13[a]
	SD	1.75	16.73	0.01[a]	10.57	2.70	8.16	0.45[a]	3.38	0.12[a]	0.10[a]

	Eigenvalue	Eu/10^{-6}	Ga/10^{-6}	Gd/10^{-6}	Hf/10^{-6}	Ho/10^{-6}	La/10^{-6}	Lu/10^{-6}	Mo/10^{-6}	Nb/10^{-6}	Nd/10^{-6}
Surface	Min	0.85	10.70	3.39	2.80	0.58	25.10	0.21	0.20	7.90	21.20
	Max	1.41	22.60	5.87	9.00	1.06	50.60	0.45	0.79	21.80	39.70
	Mean	1.18	16.66	4.87	5.34	0.87	36.46	0.35	0.45	13.30	30.14
	Median	1.17	15.80	4.94	5.10	0.90	36.70	0.37	0.42	13.10	30.60
	SD	0.13	3.54	0.68	1.42	0.14	4.97	0.07	0.16	2.88	3.90
	BGV	1.10	14.00	5.11	5.90	0.64	33.00	0.34	0.52	14.00	29.00
Core	Min	1.36[a]	15.50	5.61[a]	4.60[a]	1.02[a]	33.20	0.43[a]	0.48[a]	12.50	32.00[a]
	Max	1.46[a]	22.40	6.39[a]	5.00[a]	1.14[a]	48.60	0.51[a]	0.73[a]	15.60	34.20[a]
	Mean	1.40[a]	19.53	6.02[a]	4.76[a]	1.07[a]	42.50	0.47[a]	0.57[a]	14.53	33.15[a]
	Median	1.40[a]	20.05	6.00[a]	4.70[a]	1.07[a]	42.95	0.47[a]	0.55[a]	14.75	33.15[a]
	SD	0.03[a]	1.94	0.22[a]	0.14[a]	0.03[a]	3.80	0.02[a]	0.07[a]	0.75	0.70[a]

	Eigenvalue	Ni/10^{-6}	Pb/10^{-6}	Pr/10^{-6}	Rb/10^{-6}	Sc/10^{-6}	Sm/10^{-6}	Sn/10^{-6}	Sr/10^{-6}	Ta/10^{-6}	Tb/10^{-6}
Surface	Min	16.80	18.60	5.73	76.90	5.50	3.95	1.00	132.00	0.59	0.49
	Max	47.50	35.50	10.84	148.50	17.00	7.54	3.30	462.00	2.01	0.89
	Mean	33.01	24.64	8.25	108.65	11.59	5.81	2.41	215.80	0.99	0.74
	Median	31.00	23.20	8.43	104.40	11.20	6.00	2.30	187.00	0.99	0.76
	SD	9.00	4.75	1.08	19.79	3.22	0.76	0.63	78.70	0.25	0.11
	BGV	24.00	20.00	7.37	96.00	8.80	5.60	3.00	230.00	0.98	0.73
Core	Min	40.30	27.00	8.75[a]	115.60	10.10	6.48[a]	11.20	117.50	1.20[a]	0.87[a]
	Max	51.90	34.10	9.47[a]	157.70	29.70	6.99[a]	19.00	151.70	1.30[a]	0.96[a]
	Mean	47.59	30.25	9.13[a]	140.61	17.19	6.68[a]	15.26	128.24	1.26[a]	0.92[a]
	Median	48.15	30.40	9.17[a]	144.70	16.15	6.66[a]	15.70	123.85	1.30[a]	0.93[a]
	SD	3.54	1.70	0.21[a]	13.03	4.57	0.17[a]	1.95	9.73	0.05[a]	0.03[a]

	Eigenvalue	Th/10^{-6}	Tl/10^{-6}	Tm/10^{-6}	U/10^{-6}	V/10^{-6}	W/10^{-6}	Y/10^{-6}	Yb/10^{-6}	Zn/10^{-6}	Zr/10^{-6}
Surface	Min	6.89	0.34	0.22	1.18	57.00	0.80	17.10	1.39	42.00	104.00
	Max	18.10	0.70	0.44	2.90	126.00	4.70	28.80	2.89	124.00	362.00
	Mean	12.12	0.51	0.36	2.33	94.14	2.39	24.75	2.30	78.80	201.91
	Median	12.30	0.49	0.37	2.50	89.00	2.20	25.70	2.41	71.00	193.00
	SD	2.29	0.11	0.06	0.44	20.47	0.96	3.59	0.41	23.44	57.15
	BGV	11.50	0.30	0.15	1.90	71.00	1.50	22.00	2.20	65.00	210.00
Core	Min	15.05[a]	0.70[a]	0.43[a]	2.67[a]	106.40	6.80	16.60	2.86[a]	76.60	140.40
	Max	16.05[a]	0.87[a]	0.49[a]	2.77[a]	144.30	21.40	24.20	3.39[a]	104.70	192.30
	Mean	15.50[a]	0.81[a]	0.45[a]	2.72[a]	129.57	14.55	19.86	3.05[a]	92.58	160.28
	Median	15.50[a]	0.83[a]	0.45[a]	2.72[a]	130.80	14.50	19.45	3.05[a]	95.35	154.95
	SD	0.24[a]	0.05[a]	0.01[a]	0.03[a]	7.41	2.85	1.61	0.13[a]	9.29	12.86

SD: standard deviation, BGV: background value from Zhao and Yan (1992)

[a] Due to the lack of measurement in two cores at the National Oceanography Centre, Southampton, UK, some elements use the results measured at the ALS Minerals - ALS Chemex facility, which includes Cd, Cs, Dy, Er, Eu, Gd, Hf, Ho, Lu, Mo, Nd, Pr, Sm, Ta, Tb, Th, Tl, Tm, U, Yb.

Table 2
Categories of element distribution patterns in this study.

Patterns	Elements	Characteristics
Dual-core	Al, Be, Bi, Ti, Si, Fe, Cu, Co, Cr, Cs, Ga, In, Ni, Sc, Sn, Tl, V, W, U, Zn HREY (Gd, Tb, Dy, Ho, Er, Tm, Lu, Yb, Y)	Two higher concentration regions of these elements are present, one located at the mouth of the estuary and bay in the west, another located in clay-rich sediments in the northeast to the west of Cheju Island (concentrations are generally higher in the former area), except Si that has the opposite distribution with these two regions having lower concentration.
	K, Li, Mg, Nb, Rb, Ta, Th LREY (La, Ce, Pr, Nd, Sm, Eu)	The elements in the high concentration area in the northeast are slightly higher than those in the high concentration area near the estuary.
Single-core	As, Cd, Mo, Mn, P, Pb	These elements show high concentrations in the estuarine or coastal zone, and decrease gradually with distance offshore.
Gradient increase	Na, Ca, Sr	These elements increase significantly with distance offshore.
Multi-core	Ba	With the increase of offshore distance, the concentration of Ba decreases first, then increases to high concentration and then decreases again.
	Hf, Zr	These elements show low values in the Changjiang Estuary and Hangzhou bay, but higher concentrations in the northern Changjiang Estuary and in the central and northeast of the study area, exhibiting a complex pattern of high-low-high-low-high concentration areas from west to east.

National Oceanography Centre (Southampton).

3.2. Calculation methods

The geo-accumulation index (I_{geo}) has been widely adopted to evaluate the contamination levels of potentially toxic trace elements in sediments in relation to their corresponding background values (Muller, 1969). The I_{geo} is defined by Eq. (1) as:

$$I_{geo} = log_2 \frac{C^i}{1.5 \times C_b^i} \quad (1)$$

In which, C^i is the measured concentration of metal (or metalloid, e.g. arsenic) i, and C_b^i is the geochemical background value of i. A constant term of 1.5 is suggested to account for possible lithological variations in the background value. In this study, the background value for each trace element is taken from Zhao and Yan for East China Sea sediments (Zhao and Yan, 1994). The I_{geo} values of each trace element can be classified into seven grades: <0, No pollution; 0–1, low pollution; 1–2, partial median pollution; 2–3, median pollution; 3–4, partial serious pollution; 4–5, serious pollution; >5, extreme pollution (e.g. Duan et al., 2013; Han et al., 2017).

3.3. Mapping and statistical analysis

3.3.1. Mapping of spatial distribution

Isolines of the spatial distribution of elements, clay, silt, sand and LOI were mapped with Surfer 11.0, using the Kriging grid method to perform interpolation between data points.

3.3.2. Statistical analysis

Data were statistically analyzed using SPSS 26.0 (IBM, NY, USA).

Inter-elemental associations between major and trace elements, between elements and grain size, and between elements and LOI in the estuarine sediments were examined using Pearson correlation analysis. The Bartlett Test of Sphericity is adopted in this study, according to the Chi square statistic test value, the critical level is carried out at a 95 % confidence interval ($p < 0.05$), among which $p < 0.05$ is considered statistically significant, while $0.01 < p < 0.05$ is considered strongly statistically significant.

Cluster analysis refers to the grouping of concrete or abstract objects into classes that are composed of objects with the same types. We selected an R type clustering method in this study. The distances between classes are calculated using the Ward method, and the metric of distance is selected as the square of the Euclidean distance.

Principal Components Analysis (PCA) was applied to identify the major source(s) (and associations) of metals in this study. The PCA tries to replace the original variables with less comprehensive variables, and the integrated variables are not related to each other under the principle of minimizing the loss of data information. The significance degree of P is judged according to the Chi square value of the statistical test. When the p value is <0.05, the data are suggested to be suitable for PCA performance. Varimax with Kaiser normalization was used as the rotation method.

4. Results

4.1. Element distribution characteristics in surface and core sediments

The eigenvalues of the major and trace element contents for the surface and core sediments are presented in Table 1. Generally, the major elements Ti, Al, Fe, Mg, and K show higher values in the core sediments than in the surface sediment, which may indicate more terrigenous material input in the core sediments (as the two cores are located near to the mouth of the estuary whereas the sites for surface sediment are distributed across the wider continental shelf). With the exception of As, Hf, Sr, and Zr, most trace elements in the surface sediments show lower mean values but greater variation than in the core sediments.

The spatial distributions of major and trace elements from the 2006 sample data are shown in Fig. S3. Overall, elemental distribution can be classified into four general (spatial) patterns, as listed in Table 2.

The vertical variation of major and trace elements in cores B8 and C3 are shown in Fig. 2a. B8 shows higher concentrations of Al_2O_3, Fe_2O_3, MgO and K_2O, whereas higher concentrations of SiO_2, TiO_2, CaO, P_2O_5 are observed in C3, which is consistent with the fact that core B8 is located in an area of clay-rich sediments, whereas C3 is located in an area which is more silt-dominated (in Fig. 1). Moreover, the geographical location of core B8 is closer to the estuary than C3.

Most trace elements show higher concentrations in B8 than in C3 except As, Cu, Sr and Zr. All major and trace elements show concentrations that are relatively uniform with depth in B8, but fluctuate significantly in C3, as shown in Fig. 2b.

Two inflection points are present at depths of ~110–~130 cm and ~30–~15 cm in the two cores, and at least three stages can be identified in each core profile, based on the major and trace element profiles. First stage is from core base to a depth of ~130 cm, followed by a second stage from ~110 cm to ~30 cm. A third stage is then followed up to the sediment surface. Most major elements show an obvious decrease in core C3 during the three different stages except CaO and P_2O_5. However, the fluctuation in B8 is relatively small, especially in the second stage, and most major elements show a constant tendency, except SiO_2 and Na_2O. The continuous decrease of most major elements except CaO and P_2O_5 from ~20 cm to the surface sediment in both B8 and C3 is obvious. Most trace elements show similar trends with depth to the major elements, exhibiting the same three distinct stages with two sudden changes at depth of ~130 cm and ~30 cm. La, Ce and Y show no distinct regular

variation with depth. Some potentially harmful trace elements such as Cu, Ni, Pb, Rb, Y, Sn, Zn, Nb, W and Zr exhibit minor increases in the top 20 cm of C3, contrasting with the obvious decrease of most trace elements in the uppermost sediments of core B8.

Due to lack of sufficient sample material, measurements of some trace elements (including Be, Bi, Cd, Cs, Mn, Mo, Ta, Th, Tl, U, and the whole family of REY) were measured on different layers of the B8 core at the two laboratories used in this study. Similarly, most of these elements show relatively stable fluctuation in the second and third stages, as shown in Fig. S4.

4.2. Trace element potential risks based on Igeo

The I_{geo} values of the measured elements in surface sediments ranged from −2.38 for In to 0.97 for Tm, as shown in Table 3. The average I_{geo} values of the majority of elements are lower than 0 except Tm, Tl, and Er, ranking in a decreasing order of Tm (0.64) > Tl (0.15) > Er (0.09). Relatively higher values of I_{geo} for Tm, Tl, and Er are mainly observed near the CRE, the mouth of Hangzhou Bay, and the muddy area to the southwest of Cheju Island shown in Fig. 3. Moreover, some trace elements exhibit I_{geo} > 0 (e.g. As, Cd, Cu, Ni, Sb, V, W, Zn and so on) in

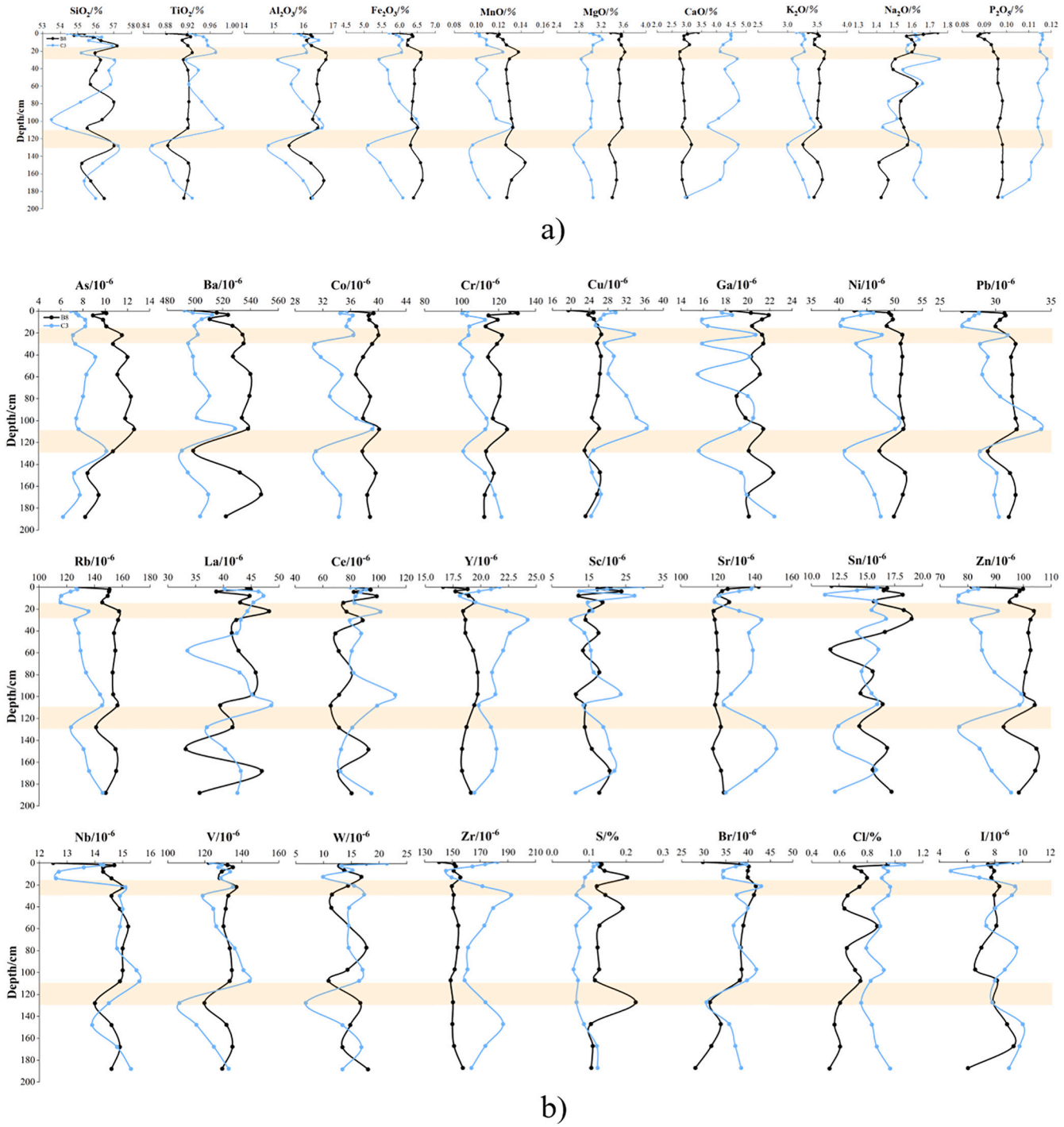

Fig. 2. a) The vertical distribution of major elements in cores B8 and C3 (black curve represents Core B8; and blue curve represents Core C3).
b) The vertical distribution of trace elements in cores B8 and C3 (black curve represents Core B8; and blue curve represents Core C3). (For interpretation of the references to color in this figure legend, the reader is referred to the web version of this article.)

Table 3
I_{geo} of trace elements in this study.

	As	Ba	Be	Bi	Cd	Ce	Co	Cr	Cs	Cu	Dy
Max	0.86	−0.40	−0.23	0.42	0.62	−0.01	0.06	0.02	0.44	0.95	−0.03
Min	−1.57	−0.65	−1.22	−1.46	−2.29	−0.98	−1.26	−1.19	−1.85	−1.91	−0.82
Ave	−0.31	−0.52	−0.63	−0.54	−0.57	−0.48	−0.43	−0.37	−0.48	−0.36	−0.28

	Er	Ga	Gd	Hf	Ho	In	La	Lu	Mo	Nb	Nd
Max	0.41	0.11	−0.38	0.02	0.14	−0.63	0.03	−0.18	0.02	0.05	−0.13
Min	−0.56	−0.97	−1.18	−1.66	−0.73	−2.38	−0.98	−1.28	−1.96	−1.41	−1.04
Ave	0.09	−0.37	−0.67	−0.78	−0.16	−1.39	−0.45	−0.59	−0.89	−0.69	−0.54

	Ni	Pb	Pr	Rb	Sc	Sm	Sn	Sr	Ta	Tb	Th
Max	0.40	0.24	−0.03	0.04	0.21	−0.16	−0.45	0.42	0.45	−0.30	0.07
Min	−1.10	−0.69	−0.95	−0.91	−1.42	−1.09	−2.17	−1.39	−1.32	−1.16	−1.32
Ave	−0.18	−0.31	−0.44	−0.43	−0.40	−0.55	−0.96	−0.75	−0.61	−0.59	−0.54

	Tl	Tm	U	V	W	Y	Yb	Zn	Zr
Max	0.64	0.97	0.03	0.24	1.06	−0.20	−0.19	0.35	0.20
Min	−0.40	−0.03	−1.27	−0.90	−1.49	−0.95	−1.25	−1.22	−1.60
Ave	0.15	0.64	−0.32	−0.21	−0.03	−0.43	−0.55	−0.37	−0.70

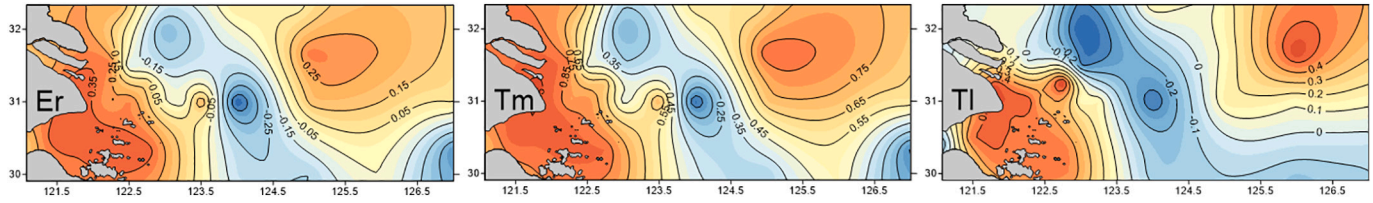

Fig. 3. The spatial distribution of I_{geo} of Er, Tm, and Tl.

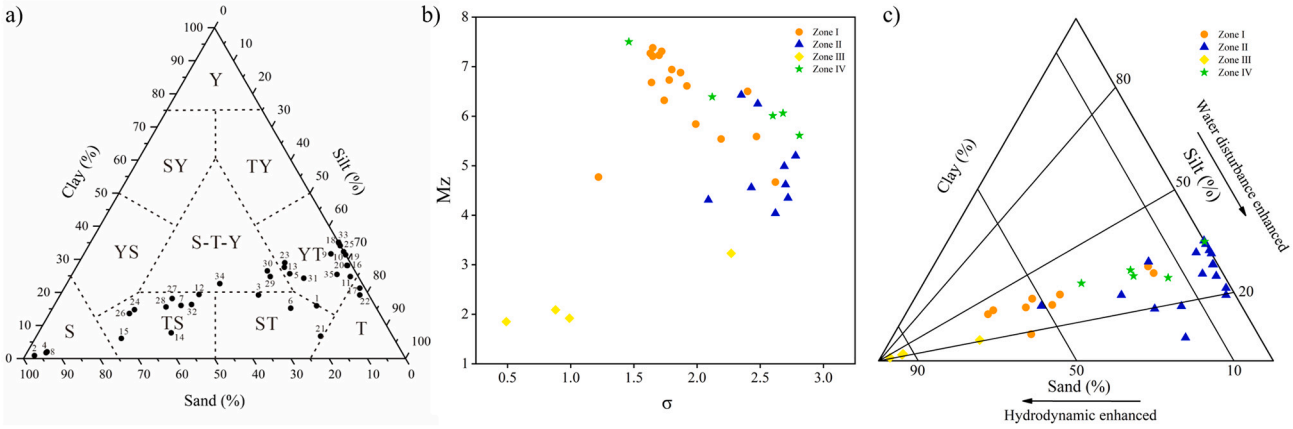

Fig. 4. a) Surface sediments classification based on Sheppard (1954); b) the Mz-σ plot of surface sediment; c) the hydrodynamics analysis in four sediments zones based on Pejurp (1988).

stations Z-10, Z-16, Z-18, Z-19, Z-20 and Z-22 at the south branch of the Changjiang River and the mouth of Hangzhou Bay, where sewage and industrial pollution discharges are common along the coast.

It is noteworthy that the I_{geo} of Tm and Er are > 0 in most stations in this area. In addition, Tm and Er are the only two members in the REE family with I_{geo} higher than 0.

For consistency with surface sediment data, only I_{geo} values of trace elements in the B8 core are calculated. In general, the I_{geo} values for B8 show similar trends to those found in surface sediments, with Tm (1.01) having the highest values, followed with Tl (0.84) > Er (0.49) > Ni (0.43) > Cs (0.45) > Cu (0.43) > Li (0.39) > Sc (0.19) > Zn (0.28) > Bi (0.28) > Cr (0.25) > Mn (0.23) > V (0.22) > Ho (0.16) > Ga (0.16) > As (0.16) > Rb (0.09) > Dy (0.08) > Co (0.07) > Fe (0.05) > Pb (0.04) > W (0.01). The remaining elements show I_{geo} values < 0. However, higher I_{geo} values for most trace elements are observed in core sediments than in the surface sediments, particularly, Tm (1.01), Tl (0.84) and Er (0.49) are found with the highest I_{geo} in core B8 compared to surface sediments.

Table 4
Relationships between trace elements and grain size in this study.

	As	Ba	Cd	Co	Cr	Cs	Cu	Ga	Hf	Mo	Nb
Sand	−0.155	−0.060	−0.731**	−0.669**	−0.810**	−0.862**	−0.805**	−0.824**	−0.207	−0.663**	−0.694**
Silt	0.163	0.042	0.741**	0.612**	0.753**	0.778**	0.782**	0.758**	0.275	0.607**	0.674**
Clay	0.104	0.089	0.559**	0.660**	0.773**	0.875**	0.691**	0.805**	0.010	0.653**	0.596**

**The correlation is significant at 0.01 level (two-tailed).
*The correlation is significant at 0.05 level (two-tailed).

4.3. Sediments classification and correlation with grain size of surface sediments

The values of grain size of the sediments are shown in Table S1. The sediments types are determined with the nomination methods proposed by Sheppard (1954) as shown in Fig. 4a. The distribution of different types of surface sediments is basically consistent with those by Shi (2021), except stations of Z-1, Z-5, Z-13, Z-30.

Four types of sedimentary zones are determined in this study according to the grain size of the sediments (in Fig. 1, Table S2). The result is consistent with previous classification (Dou, 2007; Zhang et al., 2013). The clayey-silty zone at the mouth of the CRE and Hangzhou Bay with Mz of 6.44 and σ of 1.88, shows very fine particle and high degree sorting under the relatively strong hydrodynamic and water disturbance (Fig. 4c); With the weakening of hydrodynamic and water disturbance, the sandy zone extends along the shelf of the ECS, of which the sediments show variable grain size (Mz varies between 4.04–6.63) and lowest sorting degree with an average σ of 2.54; The tidal sand ridge of the Yangtze shoal has the largest grain size with Mz of 2.27, and the weakest sorting with σ of 1.16; The grain size characteristic of the silty sand area in interridge depression of tidal current sand is similar to that of the CRE and Hangzhou Bay clayey-silty zone, with Mz of 6.31 and σ of 2.33, showing higher sorting degree than those from the tidal sand ridge of the Yangtze shoal, as shown in Fig. 4b.

The correlation between trace elements and grain size is shown in Table 4. Most elements are significantly positively correlated with fine particles < 63um, and negatively correlated with coarse particles except As, Ba, Hf and Zr, which have no obvious correlation with grain size. Grain size is the main controlling factor for the distribution of most trace elements in surface sediments in the study area. Sr is positively correlated with coarse-grained sand and negatively correlated with fine-grained silt and clay.

4.4. Inter-elemental relationships and classification

Three classes of trace elements can be determined by R cluster analysis, as shown in Fig. 5.

Type I includes Rb and Cs (alkali metals, members of the family of petrogenetic elements), Co, Cr, Ni and V (transition elements, members of ferrum earth family); Cu, Ga, Sn, Tl, Zn, Pb and Cd (thiophilic metallogenetic elements); Mo and W (belonging to W-Mo group elements); while As is a metalloid and usually act as heavy mineralizer. These elements positively correlate with Al (with $R^2 > 0.8$), but display strong negative correlation with Si, and weak to moderate negative correlation with Ca (as shown in Table 5). Clay sediments are the main hosts of these trace elements, and the dilution effect from Si and Ca is obvious. Grain size and sediment composition effects induced by the hydrodynamic environment are likely to be the main factors resulting in their "dual core" pattern. Redox conditions, and formation of secondary sulfide mineral phases, may also have an influence on their deposition since most metals including Cr (0.446), Cs (0.572), Cu (0.31), Mo (0.492), Ni (0.474), Rb (0.571), Sn (0.441), Th (0.411), Tl (0.559), U (0.549), V (0.463), W (0.306), Zn (0.406) have obvious correlation with SO_3 (Table 5).

Type II includes Zr, Hf, Nb, Ta, Th, U and ΣREY belonging to the rare and rare earth element group. Most of them are High Field Strength Elements (HFSE). These elements show correlation with Al, Si, and Ca to different degrees except Zr and Hf which show no distinct correlation with Al, Si and Ca. Nb, Ta, Th, U and REY have a strong positive correlation with Al, moderate negative correlation with Si, and weak negative correlation with Ca. These elements are distributed as the subpattern of "dual core" pattern and "multi-core" pattern. Type II may suggest elements which are mainly hosted in the aluminosilicate (silty) sediment and are diluted by both calcareous and siliceous biogenic sediments.

Type III is represented by Sr and Ba. Both Sr and Ba are alkaline-earth metals with active chemical properties and strong oxidation in aquatic environment, and also, they are biophilic elements. Usually Ca can be substituted by Sr due to isomorphism in marine authigenic calcareous minerals. Sr is the only trace element which shows robust positive correlation with Ca ($R^2 = 0.845$) (Table 5). Sr displays a gradual increase with distance offshore, which is similar to that of Ca in a "gradual increase" distribution pattern. Ba in marine sediments is usually derived from terrigenous transport, bio-enrichment and marine self-enrichment (Dickens, 2001; Gonneea and Paytan, 2006; Ni et al., 2006). The content of Ba in the bathyal sediments has a close relationship with the biological flux of the overlying water column, and can be used to restore paleoproductivity (Dean et al., 1997; McManus et al., 1998). In this study, Ba has no dependencies with other elements or even with grain size (Table 4), except for the positive correlation with Fe and Mn, and negative correlations with Hf and Zr (Table 5). Ba distributes in a unique multi-core pattern which may be due to its tendency to form authigenic minerals. For example, Ba precipitates from seawater forming biogenic barite or Ba-bearing silicate minerals and then deposits with sediments (Torres et al., 1996). In this sense, both Sr and Ba represent marine authigenic elements and distribute in a type different from other elements.

4.5. Proportion of trace element occurrence forms

The results of the BCR three-stage sequential extraction (SE) carried out on 12 surface sediments are shown in Table 6. Phases of F1, F2, F3 and F4 represent acid-exchangeable, reducible, oxidizable and residual forms respectively. Usually, the first three phases F1, F2 and F3 (which are collectively called effective states) have a stronger tendency for migration and transformation than the residue fraction. According to the proportion of elements in the different phases, the trace elements are classified into three categories: Category I includes V, Cr, Sc, Rb, Zr, Nb, Mo, Sn, Cs, Hf, Ta, Th, U, As, Tl and Ba. These are relatively non-extractable or available as the residual phase is the dominant fraction; Category II refers to REY, Co, Cu, Zn, Li and Ni. The residual phase is the main occurrence form of these elements, but the effective phase also occupies a significant proportion (19.41 %–38.38 %); Category III is mainly composed of Mn, Sr, and Pb, which mainly exist in the acid-exchangeable or reducible phases rather than in the residual phases, exhibiting active properties.

Although most trace elements are relatively non-extractable or unavailable in the sediments in the study area, elements of Tl, Er and Tm

Ni	Pb	Rb	Sn	Sr	Ta	Th	Tl	U	V	W	Zn	Zr	ΣREY
−0.811**	−0.416*	−0.798**	−0.836**	0.558**	−0.533**	−0.729**	−0.833**	−0.831**	−0.803**	−0.494**	−0.832**	−0.212	−0.625**
0.758**	0.375*	0.697**	0.774**	−0.578**	0.529**	0.668**	0.739**	0.785**	0.742**	0.534**	0.782**	0.276	0.603**
0.765**	0.424*	0.863**	0.804**	−0.395*	0.431**	0.716**	0.876**	0.763**	0.776**	0.301	0.774**	0.023	0.547**

with $I_{geo} > 0$ show medium availability. Pb and Mn are more active with availability, although the two elements show much lower I_{geo} values. Overall, the data indicate that the potential aquatic ecological risk of Tl, Er, Tm, Pb and Mn in this sea area should be monitored.

4.6. Core sediments depositional rate

^{210}Pb distributions with depth in cores B8 and C3 are shown in Fig. 6. The ^{210}Pb distribution is relatively uniform from 0 to 200 cm depth for core B8, and does not show the broadly exponential decline of excess ^{210}Pb expected in a uniformly accreting sediment column. No ^{137}Cs (determined via gamma spectrometry) was found in core B8 (for samples from 0 cm, 2 cm, 4 cm, 8 cm, 168 cm, 178 cm, 188 cm and 198 cm). ^{210}Pb was also determined in the near-surface layers of core C3, and showed a similar near-uniform distribution with depth as in core B8, although activities in core C3 were notably lower than in B8 (as observed for trace element data). Slight inflections in each ^{210}Pb profile indicate slight changes in sedimentation rate, or sediment compositional changes (e.g. the inflection in core B8 at ca. 80 cm depth corresponds to changes in major element composition at the same depth). The lack of a clear decline in ^{210}Pb activity with depth precludes accurate dating of either core section.

5. Discussion

In this study, most trace elements show slightly higher concentrations than those in sediments of marginal sea areas in China except Be, Co, Zn, Mo, In, Sn, Hf, Nb (Zhao and Yan, 1994). This is at least partly an effect of the data from Zhao and Yan, covering a wider area of the continental shelf than in the present study, but is also a consequence of lower anthropogenic trace elements flux through the estuary at that time. In comparison with sediments from China's other two major estuarine systems, the mean values of rare earth elements in the Changjiang River Estuary are higher than those from the Yellow River

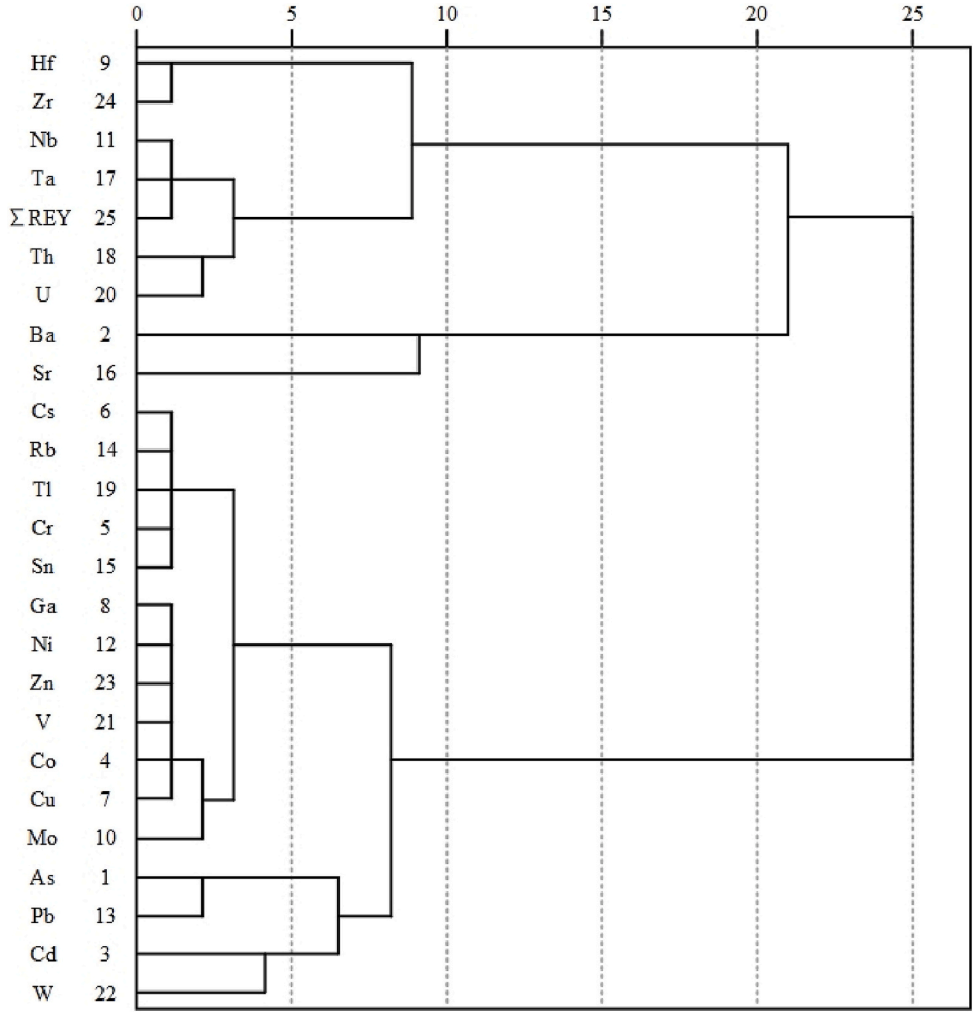

Fig. 5. R cluster analysis of trace elements.

Table 5
The inter-elemental correlations matrix.

	Al	As	Ba	Ca	Cd	Co	Cr	Cs	Cu	Fe	Ga	Hf	Mn	Mo
Al	1													
As	0.450**	1												
Ba	0.179	0.056	1											
Ca	−0.347*	−0.447**	−0.219	1										
Cd	0.741**	0.487**	0.145	−0.124	1									
Co	0.942**	0.646**	0.199	−0.501**	0.664**	1								
Cr	0.914**	0.382*	0.127	−0.323	0.769**	0.848**	1							
Cs	0.942**	0.311	0.166	−0.206	0.662**	0.857**	0.914**	1						
Cu	0.931**	0.590**	0.230	−0.318	0.874**	0.898**	0.857**	0.845**	1					
Fe	0.334*	0.152	0.447**	−0.269	0.403*	0.323	0.349*	0.343*	0.423*	1				
Ga	0.988**	0.458**	0.157	−0.332	0.731**	0.942**	0.920**	0.959**	0.924**	0.341*	1			
Hf	0.049	−0.342*	−0.439**	−0.007	0.127	−0.105	0.218	0.034	0.004	−0.128	0.046	1		
Mn	0.015	0.480**	0.345*	−0.337*	0.163	0.164	−0.003	−0.048	0.153	0.721**	0.030	−0.415*	1	
Mo	0.851**	0.648**	0.108	−0.401*	0.724**	0.877**	0.808**	0.782**	0.885**	0.243	0.865**	0.023	0.057	1
Nb	0.748**	0.201	0.088	−0.308	0.648**	0.647**	0.853**	0.739**	0.706**	0.300	0.750**	0.542**	−0.088	0.661**
Ni	0.984**	0.527**	0.211	−0.378*	0.761**	0.963**	0.926**	0.943**	0.942**	0.391*	0.984**	−0.004	0.110	0.876**
Pb	0.756**	0.834**	0.242	−0.405*	0.614**	0.872**	0.654**	0.646**	0.791**	0.163	0.757**	−0.287	0.237	0.808**
Rb	0.920**	0.311	0.199	−0.202	0.604**	0.854**	0.888**	0.986**	0.808**	0.274	0.944**	−0.019	−0.080	0.766**
S	0.477**	0.014	−0.032	−0.148	0.083	0.474**	0.446**	0.572**	0.310	0.222	0.504**	−0.095	−0.096	0.492**
SiO2	−0.693**	−0.128	−0.202	−0.180	−0.618**	−0.575**	−0.700**	−0.812**	−0.682**	−0.611**	−0.723**	0.068	−0.168	−0.532**
Sn	0.911**	0.432**	0.073	−0.213	0.731**	0.844**	0.908**	0.931**	0.867**	0.279	0.911**	0.103	−0.053	0.800**
Sr	−0.703**	−0.474**	−0.162	0.845**	−0.535**	−0.748**	−0.680**	−0.577**	−0.700**	−0.464**	−0.682**	−0.162	−0.255	−0.690**
Ta	0.575**	0.111	0.138	−0.283	0.517**	0.476**	0.726**	0.572**	0.536**	0.240	0.568**	0.595**	−0.091	0.505**
Th	0.680**	0.078	0.033	−0.172	0.491**	0.563**	0.779**	0.748**	0.603**	0.194	0.673**	0.344*	−0.274	0.569**
Tl	0.947**	0.355*	0.204	−0.192	0.678**	0.874**	0.898**	0.978**	0.860**	0.287	0.951**	−0.046	−0.075	0.802**
U	0.809**	0.095	−0.100	−0.145	0.633**	0.672**	0.857**	0.829**	0.721**	0.231	0.805**	0.480**	−0.270	0.708**
V	0.944**	0.493**	0.251	−0.384*	0.759**	0.921**	0.946**	0.938**	0.913**	0.465**	0.961**	0.057	0.156	0.857**
W	0.522**	0.421*	0.117	−0.358*	0.595**	0.535**	0.568**	0.487**	0.610**	0.424*	0.523**	0.094	0.255	0.607**
Zn	0.979**	0.475**	0.187	−0.244	0.801**	0.920**	0.910**	0.933**	0.949**	0.343*	0.968**	0.030	0.029	0.834**
Zr	0.073	−0.340*	−0.380*	−0.046	0.142	−0.081	0.252	0.050	0.025	−0.090	0.059	0.986**	−0.402*	0.037
ΣREY	0.710**	0.204	−0.021	−0.372*	0.584**	0.642**	0.843**	0.694**	0.643**	0.221	0.719**	0.590**	−0.132	0.631**

**The correlation is significant at 0.01 level (two-tailed).
*The correlation is significant at 0.05 level (two-tailed).

Estuary, but lower than those from the Pearl River Estuary (Ma et al., 2019; Yang et al., 2002).

Furthermore, the comparison to the sediments or suspended particles of main estuaries or coasts in the world previously reported is shown in Fig. 7, the REE concentration and data sources are shown in Table S3.

The REE concentrations in the bulk sediment from the CRE in this study are apparently lower than those from some big estuaries of the world, such as Nile, Mississippi, Amazon, Congo, Mekong, Ganges-Brahmaputra Estuary and so on (Bayon et al., 2015; de Oliveira et al., 2007; Dupré et al., 1996; Gaillardet et al., 1997; Hannigan et al., 2010; Ma et al., 2019; Nie et al., 2014; Stummeyer et al., 2002), but higher than those from Marabasco River Estuary, Tagus Estuary, Tintio River Estuary, Malaysia Coast, Zrmanja River estuary, Vembanad Estuary and southwest coast of India (Borrego et al., 2005; Brito et al., 2018; Censi et al., 2007; Costa et al., 2021; Fiket et al., 2017; Khadijeh et al., 2009; Manoj et al., 2016; Marmolejo-Rodríguez et al., 2007; Yang et al., 2002).

Differences in material sources, anthropogenic inputs, hydrodynamic condition, climate, and flux of sediment transport by the rivers control these concentration differences (Chi et al., 2020; Duan et al., 2019; Gao et al., 2018; Gopal et al., 2021). The large flow rate, moderate weathering rate under a subtropical monsoon climate, and a relatively short industrial history may be responsible for the medium level of elemental concentration observed in the sediments of the CRE. Previous research has suggested that most trace metals in the CRE are mainly from natural sources, except that some elements (e.g. Pb) with elevated content can be derived from anthropogenic activities (e.g., industrial effluents, mining and refining, agricultural drainage, domestic discharge, and atmospheric deposition) (Han et al., 2017). Some elements are reported as being generated in-situ due to authigenic/diagenetic processes (Higgins et al., 2018; Hüssy et al., 2021). To assess this, in this study the material sources and impacting factors of abnormally elevated trace elements were assessed through interelement correlation analysis, cluster analysis and PCA analysis. These analyses can be used to discriminate factors controlling trace element distribution and, in combination with sediment core studies, used to assess degree and timing of anthropogenic inputs. Particularly, the HREE (especially Er and Tm) are noted for their potential anthropogenic input.

5.1. Sources and impact factors of trace elements distribution

PCA analysis was performed for trace elements in the surface sediments to further evaluate their potential material sources and associations. The Kaiser-Meyer-Olkin (KMO) test statistic is 0.804, with joint probability of the Bartlett ball test of 0, which suggest that the data in this study are suitable for factor analysis. The contribution of the load and cumulative variance of the factors was obtained, as shown in Table 7.

Table 7 exhibits a 4 principal component matrix obtained after rotation and the contribution rate calculation. The cumulative variance contribution rate is 89.69 % in these 4 principal components, representing four different factors affecting the distribution characteristics of trace elements in this area.

Most trace elements (70 % above of the total) demonstrate high loads (most show correlation coefficients>0.5) on Factor 1 except As, Ba, Hf, Sr, Ta, W, Zr, which show very low or even negative loads. Combining these results with those from cluster analysis and interelement correlations, we hypothesize that Factor 1 represents a terrigenous material source carried by runoff from the Changjiang River.

As, Pb, and W show a high load on Factor 2, while Cd, Co, Cu and Mo exhibit a similar load on Factor 1 and Factor 2. We hypothesize that Factor 2 may represent impacts from mixed material sources and a sediment composition and redox effect. As most of these elements are

Nb	Ni	Pb	Rb	S	SiO2	Sn	Sr	Ta	Th	Tl	U	V	W	Zn	Zr	ΣREY
1																
0.742**	1															
0.458**	0.803**	1														
0.705**	0.920**	0.664**	1													
0.266	0.474**	0.216	0.571**	1												
−0.540**	−0.719**	−0.386*	−0.772**	−0.503**	1											
0.746**	0.919**	0.697**	0.903**	0.441**	−0.728**	1										
−0.626**	−0.721**	−0.545**	−0.530**	−0.297	0.263	−0.592**	1									
0.948**	0.574**	0.328	0.542**	0.149	−0.394*	0.590**	−0.509**	1								
0.766**	0.668**	0.379*	0.728**	0.411*	−0.561**	0.817**	−0.493**	0.690**	1							
0.692**	0.944**	0.690**	0.969**	0.559**	−0.775**	0.927**	−0.550**	0.528**	0.740**	1						
0.833**	0.774**	0.380*	0.787**	0.549**	−0.653**	0.846**	−0.559**	0.701**	0.826**	0.794**	1					
0.812**	0.972**	0.754**	0.924**	0.463**	−0.752**	0.911**	−0.720**	0.664**	0.705**	0.917**	0.786**	1				
0.491**	0.559**	0.461**	0.451**	0.306	−0.396*	0.536**	−0.583**	0.403*	0.470**	0.492**	0.491**	0.579**	1			
0.751**	0.975**	0.783**	0.913**	0.406*	−0.743**	0.927**	−0.629**	0.581**	0.685**	0.942**	0.794**	0.944**	0.532**	1		
0.577**	0.024	−0.267	−0.010	−0.082	0.053	0.125	−0.203	0.640**	0.376*	−0.018	0.490**	0.081	0.100	0.053	1	
0.923**	0.711**	0.448**	0.663**	0.258	−0.447**	0.760**	−0.650**	0.853**	0.785**	0.647**	0.831**	0.774**	0.450**	0.698**	0.621**	1

listed as compulsory detection items for marine sediment quality, factor 2 is suggested as a category which may come at least partly from anthropogenic input.

Elements with higher load on Factor 3 are mainly composed of Hf, Nb, Ta, Zr and REY. These elements are relatively stable in the marine environment, and are basically sourced from continental detrital substances (although we note possibly anthropogenic enrichments of some HREE, as discussed below). Material eroded from the OYRD is likely to be the main source of these elements.

Ba is the only element exhibiting the highest load on Factor 4. As mentioned, Ba is obviously not controlled by particle size. Besides, except a weak positive correlation (0.447 and 0.345) with Fe and Mn, it shows that Ba doesn't correlate with other elements. In marine environments, Ba is prone to form its own minerals and can be easily adsorbed by iron and manganese hydroxides. Thus, factor 4 is suggested to represent materials with marine source and authigenic enrichment.

All the four factors show negative correlation with Sr, indicating that the distribution of Sr is controlled by other factors, regarding a strong correlation between Sr and Ca (0.845) and the content decreases with the grain size, Sr indicated to represent biogenesis sources.

5.2. Sedimentary zone and the element distribution patterns

Most land sourced elements including major elements such as Al_2O_3, K_2O, FeO, MgO and TiO_2, as well as most trace elements and REY, show a dual-core distribution pattern. The two areas with relatively higher contents of elements tally with the sedimentary zone I and IV, which are located at the clayey silty area of the CRE and Hangzhou Bay, and the southwest area of Cheju Island of 125°–126°E and 31°–32°N respectively. On the contrary, the NW-SE distributed tongue-shaped area with low elements values is located in the sandy area of sedimentary zone II and III along the shelf of the ECS. Meanwhile, SiO_2, the main chemical component of sand, shows an opposite distribution pattern to the high-low value area of most major elements, indicating the impact from high sorting under strong currents. The sedimentary zones, which formed under complex hydrodynamics with multi currents (Figs. 1 and S1) dominantly control the distribution pattern of most elements. However, it should be noted that some elements are distributed under combined impact with multi sources such as Zr and Hf, with biological effect such as Sr and Ba, and with anthropogenic input such as As and Pb.

In addition, with the continuous decrease of riverine sediment input for the establishment of dams, grain for green program, rise of sea level (Cheng et al., 2023, 2022), and amplified tidal effect (Li et al., 2021; Zhu et al., 2021), the erosion of submarine delta in the CRE is serious (Cheng et al., 2022). The corresponding resuspension combined with the Estuary Turbidity Maximum (ETM) in the CRE may induce the continuous particle sorting, which may have profound long term impacts on the element distribution in the sediments and not limited, but needs further researches.

5.3. Abnormal elevation of HREE reflects anthropogenic input

To explore the reasons for the abnormally high Er and Tm concentrations observed in this study, HREE, which represents the group of heavy rare earth elements, were normalized with Post-Archean Australian Shale (PAAS) in combination with LREE, as shown in Fig. 8. In addition, the mean values of REE from sediments of the Changjiang River, Yellow River, China offshore, and the upper continental crust (UCC) of eastern China were compared.

The average concentrations of REE in this study, sampled in 2006, are lower than REE average concentrations in sediments of the lower reaches of the Changjiang River, but higher than those of the Yellow River Estuary, and higher than those of the upper continental crust from eastern China and the marginal sea areas of China. Distinctly elevated HREE concentrations are observed at sites Z-10, Z-11, Z-16, Z-18, Z-19, Z-20, Z-22, Z-25, and Z-35. It is noteworthy that most of these sites are located at the mouth of the CRE. Particularly, Tm exhibits an obvious positive anomaly. However, LREE in these sites are basically identical to

Table 6
Proportion of the different phases of trace elements (%).

Phases	V	Cr	Sc	Rb	Zr	Nb	Mo	Sn	Cs	Hf
F1	0.03	0.22	0.21	0.24	0.00	0.00	2.38	0.06	0.02	0.01
F2	4.70	4.03	0.84	1.23	0.05	0.05	1.30	0.13	0.90	0.12
F3	2.72	3.76	8.49	0.76	0.01	0.40	11.77	0.11	1.79	0.02
F4	92.55	91.99	90.46	97.77	99.94	99.54	84.55	99.70	97.29	99.85
Effective phase	7.45	8.01	8.91	4.58	0.06	0.51	15.45	0.26	2.71	0.15

Phases	Ta	Th	U	As	Tl	Ba	La	Ce	Pr	Nd
F1	0.01	0.06	2.48	1.24	0.05	0.38	2.52	2.62	2.84	3.51
F2	0.08	0.39	5.71	8.08	1.33	1.03	15.58	17.80	18.74	20.74
F3	0.03	6.31	5.48	1.13	1.27	0.53	2.70	2.79	3.55	4.06
F4	99.88	93.24	86.33	89.55	97.35	98.06	79.20	76.79	74.87	71.69
Effective phase	0.12	6.76	13.67	10.45	2.65	1.83	22.05	24.08	26.28	28.59

Phases	Sm	Eu	Gd	Tb	Dy	Ho	Er	Tm	Yb	Lu
F1	4.06	4.28	5.13	3.91	3.69	3.21	2.98	2.41	2.36	2.21
F2	24.49	24.79	29.02	25.95	25.07	20.94	19.02	16.54	15.17	13.14
F3	5.55	6.11	6.18	6.01	6.16	5.28	5.03	4.70	4.72	4.14
F4	65.90	64.82	59.67	64.13	65.08	70.57	72.97	76.36	77.75	80.50
Effective phase	34.56	35.53	38.38	34.50	34.17	30.18	26.66	23.89	22.07	19.41

Phases	Y	Co	Ni	Cu	Zn	Li	Ni	Mn	Sr	Pb
F1	3.85	4.53	2.92	1.74	1.99	2.57	2.92	40.40	41.67	2.56
F2	21.33	21.05	10.21	18.94	16.61	7.22	10.21	16.51	3.24	48.37
F3	4.29	8.88	10.25	5.62	5.85	9.96	10.25	3.83	0.52	4.30
F4	70.53	65.54	76.63	73.70	75.54	80.26	76.63	39.25	54.57	44.77
Effective phase	29.78	31.20	21.26	24.17	24.45	19.74	21.26	60.75	51.95	55.23

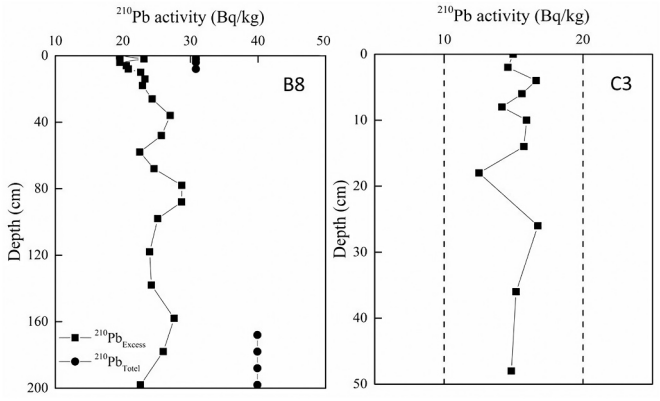

Fig. 6. ^{210}Pb activity in Core B8 and C3.

those from the sediments of the lower reaches of the Changjiang River. The different behavior between LREE and HREE in this case may be due to anthropogenic inputs.

Recently, impacts of exploitation of ion adsorption-type rare earth ores in southern China on soils and sediments have been shown (Y. Wang et al., 2022). To explore the possible input from ion adsorption-type rare earth ore mining and processing, which is wide spread in southern China and is notable for its enrichment of HREE, and its link with abnormally elevated Er and Tm observed in this study, we first examine background Er and Tm contents in soils in the Changjiang Basin, to ascertain if elevated background concentrations may be a source of the enrichments observed. Taking Er as an example, the background contents of Er are relatively low in soils in the lower reaches of the Changjiang River Delta. The contents of Er in soils from Zhejiang province, Shanghai and Jiangsu province are 2.00×10^{-6}, 2.57×10^{-6}, and 2.57×10^{-6} respectively. As a comparison, the highest contents of Er in soils are observed in Yunnan province (3.56×10^{-6}) and Guizhou province (3.44×10^{-6}) in southwestern China, Jiangxi province (3.44×10^{-6}) in eastern China and Hubei province of (3.02×10^{-6}) in central China (China National Environmental Monitoring Center, n.d.). In conclusion, natural inputs of sediments enriched in Er are highly unlikely to generate the observed Er enrichments in the study samples (Yan et al., 1997; Yang et al., 2002).

It is noteworthy that Er and Tm-related industrial activity is common in the lower reaches of the Changjiang River Delta, including companies producing rare earths, adding rare earth elements to optical fiber amplifiers (namely EDFA and TDFA respectively), and generating Er^{3+} and Tm^{3+} added laser glass, additives of alloy materials and thermoluminescent elements of calcium and thulium sulfate. Meanwhile, Er oxide is an important colorant for cheap jewelry and ceramics. The ceramics industry is traditionally developed in the Changjiang River Delta and has a long history, and Zhejiang province is the main producer of small commodities such as cheap jewelry. Er and Tm emission and pollution may occur during the production and manufacturing processes from these industries.

The PAAS normalization pattern for the residual phase of the REE in these sediments is quite similar to those from deep sea sediments which are enriched in REE and bioapatite, showing a MREE "bulge" (Lecuyer et al., 1998; Reynard et al., 1999), but without a distinct δCe negative anomaly here as shown in Fig. 8. All rare earth elements show medium activity in sediment in this study, and MREE are more active than LREE and HREE. In this case, the abnormally elevated Er and Tm in sediments should be carefully monitored, and the potential ecological risk from these sediments examined further.

5.4. Record of the trace accumulation history

Although no accurate ^{210}Pb dating results for the two cores analyzed were obtained in this study, numerous research studies on the contemporary deposition rates of fine-grained sediment in the East China Sea

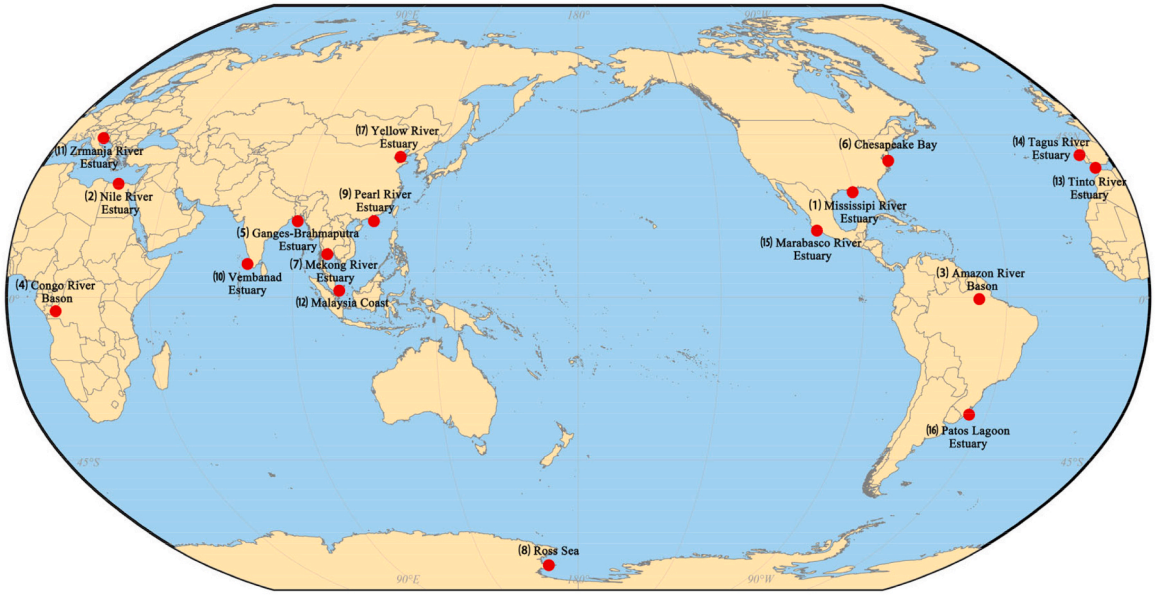

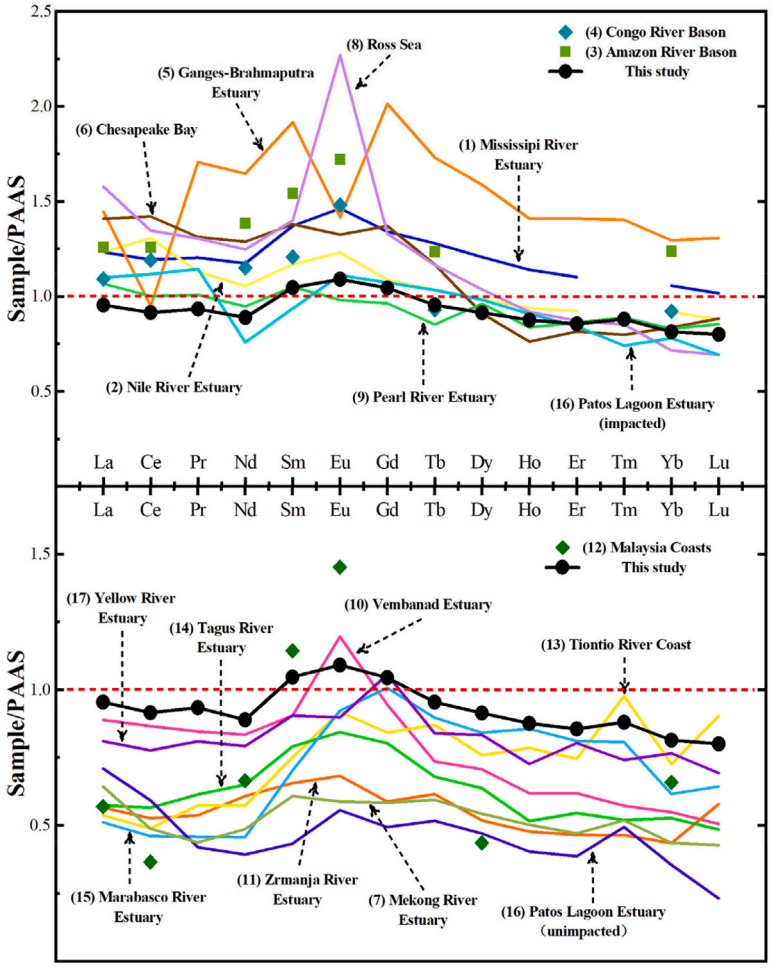

Fig. 7. Comparison of REE in Changjiang Estuary sediments with several rivers in the world (The REE concentrations of most rivers are from surface sediments, except for the Mississippi and Nile rivers, are from clay fractions. Other REE concentrations of rivers or estuaries are from suspended particulate matter, such as Amazon estuary and Congo estuary. In addition, there are also REE concentration from sediment cores, including Tintio estuary (affected and unaffected cores), Ross Sea and Patos Lagoon estuary. The whole REE concentration and data sources are shown in Table S3).

Table 7
PCA analysis.

Elements	Principle components			
	1	2	3	4
As	0.142	0.898	−0.264	−0.092
Ba	0.109	0.081	−0.204	0.955
Cd	0.521	0.589	0.235	0.075
Co	0.743	0.614	0.004	0.073
Cr	0.806	0.402	0.349	0.090
Cs	0.946	0.249	0.122	0.081
Cu	0.711	0.623	0.119	0.115
Ga	0.868	0.440	0.129	0.053
Hf	−0.034	−0.117	0.939	−0.265
Mo	0.641	0.667	0.116	−0.017
Nb	0.594	0.309	0.688	0.160
Ni	0.833	0.513	0.110	0.105
Pb	0.526	0.742	−0.186	0.078
Rb	0.950	0.220	0.064	0.105
Sn	0.873	0.365	0.193	−0.023
Sr	−0.363	−0.652	−0.331	−0.165
Ta	0.423	0.227	0.764	0.260
Th	0.735	0.073	0.467	0.054
Tl	0.942	0.279	0.050	0.096
U	0.783	0.158	0.526	−0.114
V	0.811	0.488	0.202	0.181
W	0.278	0.617	0.254	0.123
Zn	0.852	0.455	0.125	0.080
Zr	−0.023	−0.106	0.960	−0.198
ΣREY	0.573	0.303	0.699	0.029
Contribution rate of the principle components after rotation/%	44.80	21.62	18.06	5.21
Cumulative contribution rate/%	44.80	66.42	84.48	86.69

have been performed previously (Fengye et al., 2006; Hu et al., 2014; Huh and Su, 1999; Oguri et al., 2003; R. Zhang et al., 2009; Chi et al., 2020) and have suggested that the sediment accumulation rate near shore is typically 10^0–10^1 cm/a, while that on the open continental shelf is 10^{-1} cm/a (Gao, 2013). Accumulation rates of >30.00 mm/year have been observed in the Changjiang Estuary pro-delta (at the southern estuarine distributaries) and the adjacent northern part of Hangzhou Bay, in contrast to the low accumulation rates (5.00–20.00 mm/year) generally occurring in the subaqueous delta off the north branch of the Estuary. The mud deposit area occurring at the east side of the Zhejiang-Fujian coast nearly connects with the Changjiang River subaqueous delta, and shows deposition rates of >5.00 mm/year. Fine-grained sediments covering the mud are from the Changjiang River (Liu et al., 2006). We propose two possible reasons to explain the failure of dating here: 1) possibly local heterogeneity in sedimentation; 2) wide human disturbance when the surface sediment (to 200 cm) was mixed, or erosion occurred and at least part of the excess ^{210}Pb was lost. This human disturbance may be related to dredging, or sediment disturbance associated with the large-scale shipbuilding activities at Jiangnan shipyard, or the high frequency of fishing around the Zhoushan islands. Given the presence of metal enrichments within the cored sediments, it seems likely that the lack of clear decline of ^{210}Pb with depth is due to rapid sediment accumulation, rather than large-scale loss of recent sediments through erosion.

Previous work in this region has suggested a relatively stable sedimentation rate of about 3.84 cm/a (Duan et al., 2013) in the area cored. If this rate is assumed to hold for the cores in this study, the entire cored depth for B8 and C3 represents around 50 years of accumulation, which, given compositional variations within the cores (as illustrated by major element data), would explain the absence of a clear decline in ^{210}Pb activity with depth, producing a linear or erratic profile type (Cundy et al., 2003) where inflections in the ^{210}Pb profile caused by changes in sedimentation rate or compositional variability in a rapidly accreting sediment column "overwrite" the gradual exponential decline in activity expected for ^{210}Pb.

Assuming a sediment accumulation rate of 3.84 cm/a (Duan et al., 2013) or so, the depth of 130 cm corresponds to approximately 1982, a short but rapid increase of most element concentrations from 130 cm to 110 cm (Fig. 3) represents heavy metal contamination stage I (Wang, 2008). Followed with the stable decrease of element concentrations, this is due to the "conversion of farmland to forest" and the strict control policy of heavy metal pollution emission in the Changjiang River Basin.

It is interesting that there is a rapid decrease of most major elements (except Ca and P) in the top sediment layers (ca. 30 cm to core surface), which may suggest a decrease of terrigenous material input from the Changjiang River. It has been reported by a number of recent studies that the sediment discharge of the Changjiang River has reduced year by

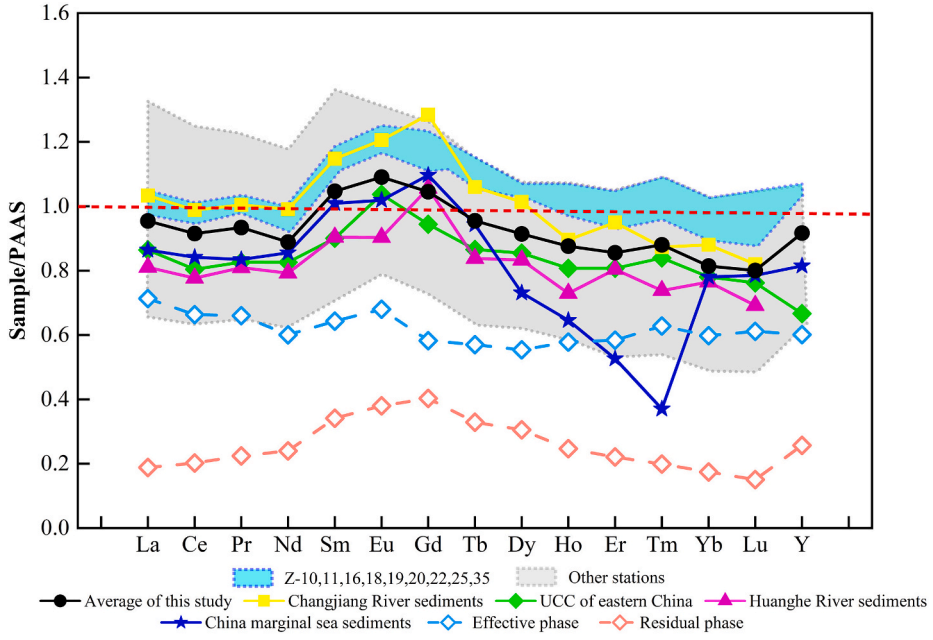

Fig. 8. Normalized REY distribution model of the surface sediments and the effective and residue forms with the comparison to previous results.
(The REY data of Changjiang River sediments and Huanghe River sediments is from Yang et al., 2002; REY data in UCC of eastern China is from Yan et al., 1997; REY data in China marginal sea sediments is from Zhao et al., 1992.)

year, and that the establishment of the TGD has aggravated this phenomenon (Cheng et al., 2023; Yang et al., 2011, 2005, 2003). Water storage in the TGD has resulted in at least a 60 % reduction of sediment transport since its construction (Xu and Milliman, 2009). The reduction of major elements including SiO_2, Al_2O_3, TiO_2, TFe, MnO_2, K_2O observed in the upper core layer can be attributed to a reduction of terrigenous input, whereas the CaO increase represents a relative increase of marine biogenic material in the sediments. P show slight decrease in the B8 core and remains unchanged in C3. It is noteworthy that some trace elements have an opposite trend in the top 30 cm of B8 and C3. For example, As, Ba, Co, Cu, Ga, Ni, Pb, Rb, Sn, Zn, Nb, Zr and Br decrease in core B8, whereas Cr, Sr, Cl and I increase, however, no distinct variation tendency is observed for La, Ce, S, W, V and Sc. It should be noted that both B8 and C3 are under the control of the ECSCC, and the consistent variation of most elements deeper than 30 cm suggests that terrigenous material transported by the CDW is the main material source for the two cores. However, with the recent decrease of terrigenous materials input from the Changjiang River Basin, a number of trace elements exhibit a decrease in the upper section of B8, whereas C3 may record an increased input of local anthropogenic pollutants or metal accumulation in the sediments.

6. Conclusion

This work has assessed the accumulation, sources and historical inputs of 25 trace elements and 15 REE in core and surface sediments of the Changjiang River Estuary and its adjacent marine area. Key conclusions are:

1) The sediments in the Changjiang River Estuary and its adjacent marine areas are mainly transported by the runoff of Changjiang River, but there are obvious trace element enrichments in the estuary areas. The mouth of the south branch of the Changjiang River and Hangzhou Bay are the two main areas controlled by deposition pattern which show elevated sedimentary concentrations of most trace elements. Medium and/or low toxic elements such Er, Tm, are dominant rather than harmful metals such As and Pb, moreover, Tl with critically elevated concentration is observed in this study as well.
2) A gradual increase of elements in the sediment cores from bottom to top is clear. It is noteworthy that at the top (0-30 cm), major elements such as SiO_2, Al_2O_3 and Fe_2O_3 are characterized by an obvious downward trend, but Ca and P expression is significantly increased, showing the impact of the completion of the Three Gorges Dam on material transport through the Changjiang River Estuary. At the same time, most of the trace elements show a decreasing trend in the upper layers of the cores, also reflecting the impact of the Three Gorges Dam, pollutant control measures, and the returning of farmland to forest. Some trace elements however, mainly in core C3, show a tendency for accumulation in the upper sediments, indicating local anthropogenic input or sedimentation effects rather than from the Changjiang Diluted Water.
3) Compared with previous research, the REE at some stations in the Changjiang River Estuary in this study show significant HREE enrichment characteristics. The proportion of HREE at several stations near the Changjiang River Estuary is higher than that at other stations located on the continental shelf, indicating anthropogenic input. The development of rare earth element processing and manufacturing industries may be the main reason for the local enrichment in the Changjiang River Estuary. The medium activity of REE in effective phases within the sediment indicates their potential availability and the need to monitor or assess potential ecological risk.

CRediT authorship contribution statement

Conceptualization, Xiaoyu Zhang; methodology, Xiaoyu Zhang, Wen Du, Zhijie Xu; software, Xiaoyu Zhang, Zhijie Xu; validation, Xiaoyu Zhang and Zhijie Xu; formal analysis, Xiaoyu Zhang, Wen Du, Zhijie Xu; resources, Weiyan Zhang, Andrew B. Cundy, Ian W. Croudace, Haiyan Jin, Jianfang Chen; data curation, Xiaoyu Zhang, Wen Du, Zhijie Xu; writing—original draft preparation, Xiaoyu Zhang, Wen Du and Zhijie Xu; writing—review and editing, Xiaoyu Zhang and Zhijie Xu; visualization, Zhijie Xu; supervision, Xiaoyu Zhang; project administration, Xiaoyu Zhang, Weiyan Zhang, Haiyan Jin, Jianfang Chen; funding acquisition, Xiaoyu Zhang. All authors have read and agreed to the published version of the manuscript.

Declaration of competing interest

The authors declare that they have no known competing financial interests or personal relationships that could have appeared to influence the work reported in this paper.

Data availability

Data will be made available on request.

Acknowledgement

This study was supported by the National Natural Science Foundation of China (41773005, 40706057) and the Scientific Research Fund of the Second Institute of Oceanography, MNR, grant no. SJ2001.

Appendix A. Supplementary data

Supplementary data to this article can be found online at https://doi.org/10.1016/j.marpolbul.2023.115082.

References

Bayon, G., Toucanne, S., Skonieczny, C., André, L., Bermell, S., Cheron, S., Dennielou, B., Etoubleau, J., Freslon, N., Gauchery, T., Germain, Y., Jorry, S.J., Ménot, G., Monin, L., Ponzevera, E., Rouget, M.L., Tachikawa, K., Barrat, J.A., 2015. Rare earth elements and neodymium isotopes in world river sediments revisited. Geochim. Cosmochim. Acta 170, 17–38. https://doi.org/10.1016/j.gca.2015.08.001.

Borrego, J., López-González, N., Carro, B., Lozano-Soria, O., 2004. Origin of the anomalies in light and middle REE in sediments of an estuary affected by phosphogypsum wastes (south-western Spain). Mar. Pollut. Bull. 49, 1045–1053. https://doi.org/10.1016/j.marpolbul.2004.07.009.

Borrego, J., López-González, N., Carro, B., Lozano-Soria, O., 2005. Geochemistry of rare-earth elements in Holocene sediments of an acidic estuary: environmental markers (Tinto River Estuary, South-Western Spain). J. Geochem. Explor. 86, 119–129. https://doi.org/10.1016/j.gexplo.2005.05.002.

Brito, P., Prego, R., Mil-homens, M., Caçador, I., Caetano, M., 2018. Sources and distribution of yttrium and rare earth elements in surface sediments from Tagus estuary, Portugal. Sci. Total Environ. 621, 317–325. https://doi.org/10.1016/j.scitotenv.2017.11.245.

Censi, P., Sprovieri, M., Saiano, F., Di Geronimo, S.I., Larocca, D., Placenti, F., 2007. The Behaviour of REEs in Thailand's Mae Klong Estuary: Suggestions From the Y/Ho Ratios and Lanthanide Tetrad Effects Thailand Gulf of, p. 71. https://doi.org/10.1016/j.ecss.2006.09.003.

Chang, P.H., Isobe, A., Kang, K.R., Ryoo, S.B., Kang, H. Suk, Kim, Y.H., 2014. Summer behavior of the Changjiang diluted water to the East/Japan Sea: a modeling study in 2003. Cont. Shelf Res. 81, 7–18. https://doi.org/10.1016/j.csr.2014.03.007.

Cheng, H.Q., Chen, W., Li, J.F., Jiang, Y.H., Hu, X., Zhang, X.L., Zhou, F.N., Hu, F.X., Stive, M.J.F., 2022. Morphodynamic changes in the Yangtze Estuary under the impact of the Three Gorges Dam, estuarine engineering interventions and climate-induced sea level rise. Earth Planet. Sci. Lett. 580 https://doi.org/10.1016/j.epsl.2022.117385.

Cheng, H., Xin, P., Liu, J., Gu, F., Shen, Q., Han, L., 2023. Morphological Evolution and Driving Factors of Tidal Flats in the Yangtze Estuary (China) During 1998–2019. Springer, Singapore. https://doi.org/10.1007/978-981-19-6138-0_101.

Chi, G., Liu, B., Hu, K., Xu, S., Wang, Z., 2020. Sedimentary records of the Yangtze Estuary over the past 70 years and their implications for provenance. Environ. Earth Sci. 79, 1–15. https://doi.org/10.1007/s12665-020-09219-5.

China National Environmental Monitoring Center, n.d. The Background Elemental Data in Soils of China.

Costa, L., Mirlean, N., Johannesson, K.H., 2021. Rare earth elements as tracers of sediment contamination by fertilizer industries in Southern Brazil, Patos Lagoon Estuary. Appl. Geochem. 129, 104965 https://doi.org/10.1016/j.apgeochem.2021.104965.

Croudace, I.W., Williams-Thorpe, O., 1988. A low dilution, wavelength-dispersive X-ray fluorescence procedure for the analysis of archaeological rock artefacts. Archaeometry 30, 227–236. https://doi.org/10.1111/j.1475-4754.1988.tb00449.x.

Cundy, A.B., Croudace, I.W., Cearreta, A., Irabien, M.J., 2003. Reconstructing historical trends in metal input in heavily-disturbed, contaminated estuaries: studies from Bilbao, Southampton Water and Sicily. Appl. Geochem. 18, 311–325. https://doi.org/10.1016/S0883-2927(02)00127-0.

de Oliveira, S.M.B., da Silva, P.S.C., Mazzilli, B.P., Favaro, D.I.T., Saueia, C.H., 2007. Rare earth elements as tracers of sediment contamination by phosphogypsum in the Santos estuary, southern Brazil. Appl. Geochem. 22, 837–850. https://doi.org/10.1016/j.apgeochem.2006.12.017.

de Souza Viana, L.M., Constantino, W.D., Tostes, E.C.L., Luze, F.H.R., de Barros Salomão, M.S.M., de Jesus, T.B., de Carvalho, C.E.V., 2023. Seasonal variation, contribution and dynamics of trace elements in the drainage basin and estuary of the Serinhaém river, BA. Mar. Pollut. Bull. 188 https://doi.org/10.1016/j.marpolbul.2023.114653.

Dean, W.E., Gardner, J.V., Piper, D.Z., 1997. Inorganic geochemical indicators of glacial-interglacial changes in productivity and anoxia on the California continental margin. Geochim. Cosmochim. Acta 61, 4507–4518. https://doi.org/10.1016/S0016-7037(97)00237-8.

Dickens, G.R., 2001. Sulfate profiles and barium fronts in sediment on the Blake Ridge: present and past methane fluxes through a large gas hydrate reservoir. Geochim. Cosmochimi. Acta 65, 529–543. https://doi.org/10.1016/S0016-7037(00)00556-1.

Dou, Y., 2007. Characteristics of Sediment Granularity, Element Geochemistry and Their Significance for Identifying Sedimentary Environment in the Contiguous Sea Areas of Changjiang River Estuary.

Du, W., Zhang, X., Ge, B., 2019. Geochemical characteristics and environmental risk assessment of antimony in surface sediments from the Yangtze River Estuary and its adjacent sea area. Bull. Sci. Technol. 35, 193–200 (in Chinese).

Duan, L., Song, J., Yuan, H., Li, X., Li, N., 2013. Spatio-temporal distribution and environmental risk of arsenic in sediments of the East China Sea. Chem. Geol. 340, 21–31. https://doi.org/10.1016/j.chemgeo.2012.12.009.

Duan, L.Q., Song, J.M., Yuan, H.M., Li, X.G., Li, N., Ma, J.K., 2014. Distribution, chemical speciation and source of trace elements in surface sediments of the Changjiang Estuary. Environ. Earth Sci. 72, 3193–3204. https://doi.org/10.1007/s12665-014-3225-6.

Duan, L., Song, J., Liang, X., Yin, M., Yuan, H., Li, X., Ren, C., Zhou, B., Kang, X., Yin, X., 2019. Dynamics and diagenesis of trace metals in sediments of the Changjiang Estuary. Sci. Total Environ. 675, 247–259. https://doi.org/10.1016/j.scitotenv.2019.04.190.

Dubiella-Jackowska, A., Polkowska, Z., Namieńnik, J., 2009. Platinum group elements in the environment: emissions and exposure. Rev. Environ. Contam. Toxicol. 199, 111–135. https://doi.org/10.1007/978-0-387-09808-1_3.

Dupré, B., Gaillardet, J., Rousseau, D., Allègre, C.J., 1996. Major and trace elements of river-borne material: the Congo Basin. Geochim. Cosmochim. Acta 60, 1301–1321. https://doi.org/10.1016/0016-7037(96)00043-9.

El Zrelli, R., Baliteau, J.Y., Yacoubi, L., Castet, S., Grégoire, M., Fabre, S., Sarazin, V., Daconceicao, L., Courjault-Radé, P., Rabaoui, L., 2021. Rare earth elements characterization associated to the phosphate fertilizer plants of Gabes (Tunisia, Central Mediterranean Sea): geochemical properties and behavior, related economic losses, and potential hazards. Sci. Total Environ. 791 https://doi.org/10.1016/j.scitotenv.2021.148268.

Essumang, D.K., Adokoh, C.K., 2011. Deposition of platinum-group metals in sediment and water bodies along the coastal belt of Ghana. Maejo Int. J. Sci. Technol. 5, 331–349.

Essumang, D.K., Adokoh, C.K., Boamponsem, L., 2010. Levels of platinum group metals in selected species (Sarotherodon melanotheron, Chonophorus lateristriga, Macrobrachium vollenhovenii and Crassostrea tulipa) in some estuaries and lagoons along the coast of Ghana. ScientificWorldJournal. 10, 1971–1987. https://doi.org/10.1100/tsw.2010.197.

Fengye, L., Xuegang, L., Jinming, S., Guizhi, W., Peng, C., Shu, G., 2006. Sediment flux and source in northern Yellow Sea by210Pb technique. Chin. J. Oceanol. Limnol. 24, 255–263. https://doi.org/10.1007/bf02842625.

Fiket, Ž., Mikac, N., Kniewald, G., 2017. Influence of the geological setting on the REE geochemistry of estuarine sediments: a case study of the Zrmanja River estuary (eastern Adriatic coast). J. Geochem. Explor. 182, 70–79. https://doi.org/10.1016/j.gexplo.2017.09.001.

Fiket, Ž., Ivanić, M., Turk, M.F., Mikac, N., Kniewald, G., 2018. Distribution of trace elements in waters of the Zrmanja River Estuary (Eastern Adriatic Coast, Croatia). Croat. Chem. Acta 91, 29–41. https://doi.org/10.5562/cca3202.

Flynn, W.W., 1968. The determination of low levels of polonium-210 in environmental materials. Anal. Chim. Acta 43, 221–227. https://doi.org/10.1016/S0003-2670(00)89210-7.

Folk, R.L., Folk, R.L., 1957. A study in the significance of grain size parameters. J. Sediment. Petrol. 27, 3–26.

Gaillardet, J., Dupré, B., Allègre, C.J., Négrel, P., 1997. Chemical and physical denudation in the Amazon River Basin. Chem. Geol. 142, 141–173. https://doi.org/10.1016/S0009-2541(97)00074-0.

Gao, S., 2013. Holocene sedimentary systems over the Bohai, Yellow and East China Sea region: recent progress in the study of process-product relationships. Acta Sedimentol. Sin. 31, 845–855.

Gao, J., Shi, H., Dai, Z., Mei, X., Zong, H., Yang, H., Hu, L., Li, S., 2018. Linkages between the spatial toxicity of sediments and sediment dynamics in the Yangtze River Estuary and neighboring East China Sea. Environ. Pollut. 233, 1138–1146. https://doi.org/10.1016/j.envpol.2017.10.023.

Gonneea, M.E., Paytan, A., 2006. Phase associations of barium in marine sediments. Mar. Chem. 100, 124–135. https://doi.org/10.1016/j.marchem.2005.12.003.

Gopal, V., Krishnamurthy, R.R., Sreeshma, T., Chakraborty, P., Nathan, C.S., Kalaivanan, R., Anshu, R., Magesh, N.S., Jayaprakash, M., 2021. Effect of a tropical cyclone on the distribution of heavy metals in the marine sediments off Kameswaram, Southeast coast of India. Mar. Pollut. Bull. 171, 112741 https://doi.org/10.1016/j.marpolbul.2021.112741.

Guo, Y., Yang, S., 2016. Heavy metal enrichments in the Changjiang (Yangtze River) catchment and on the inner shelf of the East China Sea over the last 150years. Sci. Total Environ. 543, 105–115. https://doi.org/10.1016/j.scitotenv.2015.11.012.

Han, D., Cheng, J., Hu, X., Jiang, Z., Mo, L., Xu, H., Ma, Y., Chen, X., Wang, H., 2017. Spatial distribution, risk assessment and source identification of heavy metals in sediments of the Yangtze River Estuary, China. Mar. Pollut. Bull. 115, 141–148. https://doi.org/10.1016/j.marpolbul.2016.11.062.

Hannigan, R., Dorval, E., Jones, C., 2010. The rare earth element chemistry of estuarine surface sediments in the Chesapeake Bay. Chem. Geol. 272, 20–30. https://doi.org/10.1016/j.chemgeo.2010.01.009.

Hao, Y., Guo, Z., Yang, Z., Fan, D., Fang, M., Li, X., 2008. Tracking historical lead pollution in the coastal area adjacent to the Yangtze River Estuary using lead isotopic compositions. Environ. Pollut. 156, 1325–1331. https://doi.org/10.1016/j.envpol.2008.02.023.

He, Z., Li, F., Dominech, S., Wen, X., Yang, S., 2019. Heavy metals of surface sediments in the Changjiang (Yangtze River) Estuary: distribution, speciation and environmental risks. J. Geochem. Explor. 198, 18–28. https://doi.org/10.1016/j.gexplo.2018.12.015.

Higgins, J.A., Bla, C.L., Lundstrom, E.A., Santiago-ramos, D.P., Akhtar, A.A., Cru, A., Bialik, O., Holmden, C., Bradbury, H., 2018. Mineralogy, early marine diagenesis, and the chemistry of shallow-water carbonate sediments. Geochim. Cosmochim. Acta 220, 512–534. https://doi.org/10.1016/j.gca.2017.09.046.

Hu, G., Li, A., Liu, J., Xu, G., Mei, X., Kong, X., 2014. High resolution records of flood deposition in the mud area off the Changjiang River mouth during the past century. Chin. J. Oceanol. Limnol. 32, 909–920. https://doi.org/10.1007/s00343-014-3244-x.

Hu, X., Shi, X., Su, R., Jin, Y., Ren, S., Li, X., 2022. Spatiotemporal patterns and influencing factors of dissolved heavy metals off the Yangtze River Estuary, East China Sea. Mar. Pollut. Bull. 182 https://doi.org/10.1016/j.marpolbul.2022.113975.

Huh, C.A., Su, C.C., 1999. Sedimentation dynamics in the East China Sea elucidated from 210Pb, 137Cs and 239,240Pu. Mar. Geol. 160, 183–196. https://doi.org/10.1016/S0025-3227(99)00020-1.

Hüssy, K., Limburg, K.E., De Pontual, H., Thomas, O.R.B., Cook, K., Heimbrand, Y., Blass, M., Sturrock, A.M., Hüssy, K., Limburg, K.E., De Pontual, H., Thomas, O.R.B., Cook, K., Heimbrand, Y., Blass, M., Sturrock, A.M., Element, T., Heimbrand, Y., Cook, P.K., 2021. Trace element patterns in otoliths: the role of biomineralization. Rev. Fish. Sci. Aquac. 29, 445–477. https://doi.org/10.1080/23308249.2020.1760204.

Khadijeh, R.E.S., Elias, S.B., Wood, A.K., Reza, A.M., 2009. Rare earth elements distribution in marine sediments of Malaysia coasts. J. Rare Earths 27, 1066–1071. https://doi.org/10.1016/S1002-0721(08)60390-7.

Kimbrough, K.L., Commey, S., Apeti, D.A., Lauenstein, G.G., 2010. Chemical contamination assessment of the Hudson-Raritan Estuary as a result of the attacks on the World Trade Center: analysis of trace elements. Mar. Pollut. Bull. 60, 2289–2296. https://doi.org/10.1016/j.marpolbul.2010.07.009.

Komendova, R., 2020. Recent advances in the preconcentration and determination of platinum group metals in environmental and biological samples. Trends Anal. Chem. 122, 115708 https://doi.org/10.1016/j.trac.2019.115708.

Kulaksiz, S., Bau, M., 2007. Contrasting behaviour of anthropogenic gadolinium and natural rare earth elements in estuaries and the gadolinium input into the North Sea. Earth Planet. Sci. Lett. 260, 361–371. https://doi.org/10.1016/j.epsl.2007.06.016.

Lecuyer, C., Grandjean, P., Barrat, J.A., Nolvak, J., Emig, C., Paris, F., Robardet, M., 1998. δ18O and REE contents of phosphatic brachiopods: a comparison between modern and lower Paleozoic populations. Geochim. Cosmochim. Acta. 62, 2429–2436. https://doi.org/10.1016/S0016-7037(98)00170-7.

Li, L., Jiang, M., Liu, Y., Shen, X., 2019. Heavy metals inter-annual variability and distribution in the Yangtze River estuary sediment, China. Mar. Pollut. Bull. 141, 514–520. https://doi.org/10.1016/j.marpolbul.2019.03.008.

Li, Y., Wang, Y.P., Zhu, Q., Limaye, A.B., Wu, H., 2021. Roles of advection and sediment resuspension-settling in the turbidity maximum zone of the Changjiang Estuary, China. Cont. Shelf Res. 229, 104559 https://doi.org/10.1016/j.csr.2021.104559.

Liu, J.P., Li, A.C., Xu, K.H., Velozzi, D.M., Yang, Z.S., Milliman, J.D., DeMaster, D.J., 2006. Sedimentary features of the Yangtze River-derived along-shelf clinoform deposit in the East China Sea. Cont. Shelf Res. 26, 2141–2156. https://doi.org/10.1016/j.csr.2006.07.013.

Liu, R., Men, C., Liu, Y., Yu, W., Xu, F., Shen, Z., 2016. Spatial distribution and pollution evaluation of heavy metals in Yangtze estuary sediment. Mar. Pollut. Bull. 110, 564–571. https://doi.org/10.1016/j.marpolbul.2016.05.060.

Liu, M., Chen, J., Sun, X., Hu, Z., Fan, D., 2019. Accumulation and transformation of heavy metals in surface sediments from the Yangtze River estuary to the East China Sea shelf. Environ. Pollut. 245, 111–121. https://doi.org/10.1016/j.envpol.2018.10.128.

Ma, L., Dang, D.H., Wang, W., Evans, R.D., Wang, W.X., 2019. Rare earth elements in the Pearl River Delta of China: potential impacts of the REE industry on water,

suspended particles and oysters. Environ. Pollut. 244, 190–201. https://doi.org/10.1016/j.envpol.2018.10.015.
Manoj, M.C., Thakur, B., Prasad, V., 2016. Rare earth element distribution in tropical coastal wetland sediments: a case study from Vembanad estuary, southwest India. Arab. J. Geosci. 9, 1–11. https://doi.org/10.1007/s12517-015-2246-0.
Marmolejo-Rodríguez, A.J., Prego, R., Meyer-Willerer, A., Shumilin, E., Sapozhnikov, D., 2007. Rare earth elements in iron oxy-hydroxide rich sediments from the Marabasco River-Estuary System (pacific coast of Mexico). REE affinity with iron and aluminium. J. Geochem. Explor. https://doi.org/10.1016/j.gexplo.2007.05.003.
McManus, J., Berelson, W.M., Klinkhammer, G.P., Johnson, K.S., Coale, K.H., Anderson, R.F., Kumar, N., Burdige, D.J., Hammond, D.E., Brumsack, H.J., McCorkle, D.C., Rushdi, A., 1998. Geochemistry of barium in marine sediments: implications for its use as a paleoproxy. Geochim. Cosmochim. Acta 62, 3453–3473. https://doi.org/10.1016/s0016-7037(98)00248-8.
Monteiro, C.E., Santos, M.C., Caetano, M., 2017. Platinum-Group Elements in Portuguese Aquatic Systems: The (Un)known Data and Future Research.
Muller, G., 1969. Index of geoaccumulation in sediments of the Rhine River. GeoJournal 2, 108–118.
Ni, J., Zhang, M., Zhou, H., 2006. Biogenetic barium distribution in Equatorial northeastern Pacific sediments. Mar. Geol. Quat. Geol. 26, 49–54.
Nie, Y., Liu, X., Emslie, S.D., 2014. Distribution and sources of rare earth elements in ornithogenic sediments from the Ross Sea region, Antarctica. Microchem. J. 114, 247–260. https://doi.org/10.1016/j.microc.2014.01.010.
Oguri, K., Matsumoto, E., Yamada, M., Saito, Y., Iseki, K., 2003. Sediment accumulation rates and budgets of depositing particles of the East China Sea. Deep. Res. Part II Top. Stud. Oceanogr. 50, 513–528. https://doi.org/10.1016/S0967-0645(02)00465-4.
Pejurp, M., 1988. The triangular diagram used for classification of estuarine sediments: a new approach. In: Tide-influenced Sediment. Environ. Facies. Reidel, Dordr, pp. 289–300.
Piarulli, S., Hansen, B.H., Ciesielski, T., Zocher, A.L., Malzahn, A., Olsvik, P.A., Sonne, C., Nordtug, T., Jenssen, B.M., Booth, A.M., Farkas, J., 2021. Sources, distribution and effects of rare earth elements in the marine environment: current knowledge and research gaps. Environ. Pollut. 291 https://doi.org/10.1016/j.envpol.2021.118230.
Quevauviller, P., Rauret, G., López-Sánchez, J.F., Rubio, R., Ure, A., Muntau, H., 1997. Certification of trace metal extractable contents in a sediment reference material (CRM 601) following a three-step sequential extraction procedure. Sci. Total Environ. 205, 223–234. https://doi.org/10.1016/S0048-9697(97)00205-2.
Rauret, G., López-Sánchez, J.F., Sahuquillo, A., Rubio, R., Davidson, C., Ure, A., Quevauviller, P., 1999. Improvement of the BCR three step sequential extraction procedure prior to the certification of new sediment and soil reference materials. J. Environ. Monit. 1, 57–61. https://doi.org/10.1039/a807854h.
Reynard, B., Lécuyer, C., Grandjean, P., 1999. Crystal-chemical controls on rare-earth element concentrations in fossil biogenic apatites and implications for paleoenvironmental reconstructions. Chem. Geol. 155, 233–241. https://doi.org/10.1016/S0009-2541(98)00169-7.
Sheppard, F.P., 1954. Nomenclature based on sand-silt-clay ratios. Geology 24, 151–158.
Shi, X., 2021. Sediment Type Map of the Bohai Sea, Yellow Sea and East China Sea.
Song, H., Yue, Z., Wei, S., Qiuyan, C., 2020. Environmental chemical behaviors of platinum group elements in aquatic environment (in Chinese). Environ. Chem. 39, 2055–2064. https://doi.org/10.7524/j.issn.0254-6108.2019053102.
Stummeyer, J., Marchig, V., Knabe, W., 2002. The composition of suspended matter from Ganges-Brahmaputra sediment dispersal system during low sediment transport season. Chem. Geol. 185, 125–147. https://doi.org/10.1016/S0009-2541(01)00396-5.
Su, J., Yuan, Y., 2005. Offshore Hydrology in China. China Ocean Press, Beijing.
Torres, M.E., Brumsack, H.J., Bohrmann, G., Emeis, K.C., 1996. Barite fronts in continental margin sediments: a new look at barium remobilization in the zone of sulfate reduction and formation of heavy barites in diagenetic fronts. Chem. Geol. 127, 125–139. https://doi.org/10.1016/0009-2541(95)00090-9.
Trifuoggi, M., Donadio, C., Ferrara, L., Stanislao, C., Toscanesi, M., Arienzo, M., 2018. Levels of pollution of rare earth elements in the surface sediments from the Gulf of Pozzuoli (Campania, Italy). Mar. Pollut. Bull. 136, 374–384. https://doi.org/10.1016/j.marpolbul.2018.09.034.
Ure, A.M., Quevauviller, P.H., Muntau, H., Griepink, B., 1993. Speciation of heavy metals in soils and sediments. An account of the improvement and harmonization of extraction techniques undertaken under the auspices of the BCR of the Commission of the European Communities. Int. J. Environ. Anal. Chem. 51, 135–151. https://doi.org/10.1080/03067319308027619.
Wang, B., 2008. Study on Environmental Geochemistry of Heavy Metals in Sediments of Changjiang Estuary and Adjacent Area (in Chinese).
Wang, R., Zhang, C., Huang, X., Zhao, L., Yang, S., Struck, U., Yin, D., 2020. Distribution and source of heavy metals in the sediments of the coastal East China sea: geochemical controls and typhoon impact. Environ. Pollut. 260, 113936 https://doi.org/10.1016/j.envpol.2020.113936.
Wang, Z., Shu, J., Wang, Zhaoru, Qin, X., Wang, S., 2022a. Geochemical behavior and fractionation characteristics of rare earth elements (REEs) in riverine water profiles and sentinel clam (Corbicula fluminea) across watershed scales: insights for REEs monitoring. Sci. Total Environ. 803, 150090 https://doi.org/10.1016/j.scitotenv.2021.150090.
Wang, Y., Wang, G., Sun, M., Liang, X., He, H., Zhu, J., Takahashi, Y., 2022b. Environmental risk assessment of the potential "Chemical Time Bomb" of ion-adsorption type rare earth elements in urban areas. Sci. Total Environ. 822, 153305 https://doi.org/10.1016/j.scitotenv.2022.153305.
Xu, K., Milliman, J.D., 2009. Seasonal variations of sediment discharge from the Yangtze River before and after impoundment of the Three Gorges Dam. Geomorphology 104, 276–283. https://doi.org/10.1016/j.geomorph.2008.09.004.
Yan, M., Chi, Q., Gu, T., Wang, C., 1997. Chemical composition of upper crust in eastern China. Sci. China. Ser. D Earth Sci. 05, 530–539 (in Chinese).
Yang, S.Y., Jung, H.S., Choi, M.S., Li, C.X., 2002. The rare earth element compositions of the Changjiang (Yangtze) and Huanghe (Yellow) river sediments. Earth Planet. Sci. Lett. 201, 407–419. https://doi.org/10.1016/S0012-821X(02)00715-X.
Yang, S.L., Belkin, I.M., Belkina, A.I., Zhao, Q.Y., Zhu, J., Ding, P.X., 2003. Delta response to decline in sediment supply from the Yangtze River: evidence of the recent four decades and expectations for the next half-century. Estuar. Coast. Shelf Sci. 57, 689–699. https://doi.org/10.1016/S0272-7714(02)00409-2.
Yang, S.L., Zhang, J., Zhu, J., Smith, J.P., Dai, S.B., Gao, A., Li, P., 2005. Impact of dams on Yangtze River sediment supply to the sea and delta intertidal wetland response. J. Geophys. Res. Earth Surf. 110, 1–12. https://doi.org/10.1029/2004JF000271.
Yang, Z., Wang, Y., Shen, Z., Niu, J., Tang, Z., 2009. Distribution and speciation of heavy metals in sediments from the mainstream, tributaries, and lakes of the Yangtze River catchment of Wuhan, China. J. Hazard. Mater. 166, 1186–1194. https://doi.org/10.1016/j.jhazmat.2008.12.034.
Yang, S.L., Milliman, J.D., Li, P., Xu, K., 2011. 50,000 dams later: erosion of the Yangtze River and its delta. Glob. Planet. Chang. 75, 14–20. https://doi.org/10.1016/j.gloplacha.2010.09.006.
Zhang, R., Pan, S., Wang, Y., 2009a. Distribution characteristics and deposition rate of 210Pb in the subaqueous delta of Yangtze River Estuary. Acta Sedimentol. Sin. 27, 704–713.
Zhang, X., Zhang, F., Gao, A., Zhang, W., 2009b. Source tracing implication of Pt and Pd fractionation in the surface sediment of continental shelf around Changjiang Estuary. Earth Sci. J. China Univ. Geosci. 34, 604–612.
Zhang, W., Zhang, X., Jin, H., Feng, X., Yao, X., Gao, W., Zhang, F., Gao, A., 2013. Depositional dynamic environment and provenance analysis of the Yangtze Estuary-Hangzhou Bay and its adjacent waters. Acta Geograph. Sin. 68 (in Chinese).
Zhao, Y., Yan, M., 1992. Comparison of chemical element abundance in sediments of Yellow River, Yangtze River and shallow sea of China. Chinese Sci. Bull. 13, 1202–1204 (in Chinese).
Zhao, Y., Yan, M., 1994. Geochemistry of Sediments in Chinese Shallow Sea.
Zhu, C., Guo, L., van Maren, D.S., Wang, Z.B., He, Q., 2021. Exploration of decadal tidal evolution in response to morphological and sedimentary changes in the Yangtze Estuary. J. Geophys. Res. Ocean. 126, 1–19. https://doi.org/10.1029/2020JC017019.
Zhuang, W., Liu, Y., Tang, L., Yue, W., Liu, J., Ren, Y., Wang, X., Xu, S., Tai, S., Zhang, J., Zheng, Y., Guo, F., Wang, Q., Song, J., Duan, L., Chen, Q., 2019. Thallium concentrations, sources and ecological risk in the surface sediments of the Yangtze Estuary and its adjacent east China marginal sea: a baseline study. Mar. Pollut. Bull. 138, 206–212. https://doi.org/10.1016/j.marpolbul.2018.11.049.